

**DEVELOPMENT OF A NOVEL CELL TRACTION FORCE TRANSDUCER
BASED ON CHOLESTERYL ESTER LIQUID CRYSTALS**

**Characterisation, quantification and evaluation of a cholesteryl ester liquid
crystal based single cell force transducer system**

Chin Fhong SOON

**Submitted for the degree
of Doctor of Philosophy**

School of Life Sciences

University of Bradford

2011

ABSTRACT

Development of a novel cell traction force transducer based on cholesteryl ester liquid crystals

CHIN FHONG SOON

Keywords: cholesteryl ester liquid crystals, cell force transducer, cell traction force mapping, lyotropic liquid crystals.

Abstract:

In biomechano-transducing, cellular generated tension can be measured by soft substrates based on polymers but these techniques are limited either by spatial resolution or ability to detect localised cell traction forces (CTF) due to their non-linear viscous behaviour under shear rates. A newly developed cell traction force transducer system based on cholesteryl ester lyotropic liquid crystals (LCTFT) was developed to sense localised traction forces of human keratinocyte cell lines (HaCaTs), in which the length of the deformation line induced represents the intensity of the CTF exerted. The physical properties of the cholesteryl ester based lyotropic liquid crystals (LLC) were characterised by using polarising microscopy, rheology, atomic force microscopy (AFM) based nano-indentation, spherical indentation, and micro-tensile tests. The interactions of LLC with cells were studied by using cell viability studies, cytochemical treatments, widefield surface plasmon resonance (WSPR) microscopy and various immuno-staining techniques. The results show that LLC is thermally stable (0 - 50 °C) and linearly viscoelastic below 10 % shear strain at shear rates of $< 1 \text{ s}^{-1}$. AFM nano and spherical indentations show a good agreement on the Young's modulus of both determined at $\sim 110 \text{ kPa}$ which is close to the elastic modulus of the epidermis. The Poisson's ratio of LLC was determined at ~ 0.58 by using micro tensile tests. The biophysical interaction studies indicated that LLC is biocompatible and allowed cell attachment. Cell relaxation technique by cytochalasin-B treatment suggested that the attachment and contraction of cells on LLC was due to the contractile activity of actin cytoskeletons that are mediated by focal adhesions. The staining experiments showed that cells consistently expressed the same suites of integrins ($\alpha 2$, $\alpha 3$, $\alpha 5$ and $\beta 1$) and ECM proteins (collagen type IV, laminin and fibronectin) on both glass and LLC coated substrates. Interfacial interaction of cells with LLC observed via the staining of actin and vinculin, and WSPR imaging suggest the association of marginal actin filaments and focal adhesions in attaching HaCaT cells to the LLC. Linear static analysis applied in the Finite Element model of focal adhesion-LC confirmed the compressive force patterns induced by cells. By applying cell relaxation techniques and Hooke's theorem, the force-deformation relationships of the LLC were derived and used for direct quantification of CTF in culture. The sensitivity of the LCTFT was implied by a wide range of CTF (10 - 140 nN) measured at high resolutions ($\sim 2 \mu\text{m}$). Nonetheless, a custom-built cell traction force measurement and mapping software (CTFM) was developed to map CTF of single cells. Reliability of the LCTFT was evaluated by using a known pharmacological active cytokine, TGF- $\beta 1$, in inducing contraction of human keratinocytes. This study inferred internal consistency and repeatability of the LCTFT in sensing contraction responses of HaCaT cells in a concentration dependent manner of TGF- $\beta 1$. The overall LCTFT and CTFM software had shown good potential for use in the study of contraction and migration of keratinocytes.

LIST OF CONTENTS

ABSTRACT.....	i
ACKNOWLEDGEMENT.....	ii
DEDICATION PAGE.....	iii
LIST OF ASSOCIATED PUBLICATION.....	iv
LIST OF CONTENTS.....	v
LIST OF FIGURES.....	ix
LIST OF TABLES.....	xxiv
LIST OF ABBREVIATIONS AND SYMBOLS.....	xxv
1 INTRODUCTION.....	1
1.1 Research Background	2
1.2 Cellular Adhesion, Contraction and the Measurements of Cell Traction Force.....	6
1.2.1 Epidermal Tissue	6
1.2.2 Cellular Adhesion	8
1.2.3 Integrin Receptors and Focal Adhesion	14
1.2.4 Polymerisation of Actin Filaments and Generation of Traction Force	16
1.2.5 Force Sensor Based on Silicon Sheet	24
1.2.6 Force Sensor Based on a Collagen Lattice	26
1.2.7 Force Sensor Based on Displacements of Markers in Soft Substrates	27
1.2.8 Force Sensor Based on Micro-Pillars and Micro-Patterns.....	28
1.3 Introduction to Liquid Crystals	34
1.3.1 Types of Liquid Crystals.....	35
1.3.2 Classification of Mesophases and Associated Birefringence Texture	39

1.3.3	Elasticity Theory of Chiral Nematic Liquid Crystals	44
1.3.4	Application of Liquid Crystals in Bio-Sensing.....	47
1.3.5	Viscoelasticity of Lyotropic Liquid Crystals	49
1.4	Selection of Cell Type and Requirements of Cell Traction Force Sensor	50
1.5	Hypothesis of the Research	52
1.6	Aim and Objectives of the Research.....	53
1.7	Thesis Organisation	54
2	PHYSICAL PROPERTIES: CHARACTERISATION OF CHOLESTERYL ESTER BASED LYOTROPIC LIQUID CRYSTALS	56
2.1	Introduction	57
2.2	Material and Methods.....	58
2.2.1	Preparation of Cholesteric and Nematic Liquid Crystals	58
2.2.2	Thermal and Liquid Crystalline Phase Analysis.....	60
2.2.3	Preparation of Liquid Crystal Substrate for Liquid Crystalline Study	61
2.2.4	Preparation of Liquid Crystal Gel for Rheological Test.....	62
2.2.5	Amplitude and Frequency Sweep Tests.....	62
2.2.6	Preparation of Human Keratinocyte Cell Lines.....	63
2.2.7	Culturing Cells on the Liquid Crystal Substrates.....	64
2.2.8	Characterising the Time-Dependent Viscoelasticity and Viscosity of the Liquid Crystal In-Situ	64
2.2.9	Determining Young's modulus of the Liquid Crystals.....	67
2.2.10	Measurements of Poisson's Ratio of the Liquid Crystals.....	73
2.2.11	Statistical Analysis.....	76

2.3	Results and Discussion.....	77
2.3.1	Temperature Stability of the Liquid Crystals	77
2.3.2	Identification of the Liquid Crystalline Phase	81
2.3.3	Stabilisation of Shear Modulus at Low Shear Strain.....	86
2.3.4	Shear Rate Dependent Shear Modulus of the Lyotropic Liquid Crystals ..	91
2.3.5	Analysis on the Structural Changes of the Liquid Crystal Substrates Cultured with Cells.....	96
2.3.6	Viscoelasticity and Viscosity of the Time-Dependent Liquid crystals In-Situ	102
2.3.7	The Young's Modulus of Liquid Crystals Determined by Using AFM Nano- Indentation	107
2.3.8	The Young's Modulus of the Liquid Crystals Determined by Spherical Indentation	109
2.3.9	Effects of Incubation Time to the Young's Modulus of the Liquid Crystals	113
2.3.10	Poisson's Ratio of the Liquid Crystals	114
2.4	Summary.....	121
3	BIOPHYSICAL INTERACTIONS OF CELLS AND LIQUID CRYSTALS	122
3.1	Introduction	123
3.2	Material and Methods.....	124
3.2.1	The Cell Viability Studies.....	124
3.2.2	Treatment with Cytochalasin B and EDTA-Trypsin.....	125
3.2.3	Fluorescence Staining of Cytoskeleton, Vinculin and Integrins.....	127
3.2.4	Immunoperoxidase Staining of Laminin	128

3.2.5	Immunoperoxidase Staining of Collagen Type IV	129
3.2.6	Immunofluorescence Staining of Fibronectin	130
3.2.7	Fluorescence Microscopy	130
3.2.8	Widefield Surface Plasmon Imaging of Cell-Liquid Crystals Interface.....	131
3.2.9	Statistical Analysis.....	133
3.3	Results and Discussion.....	134
3.3.1	Affinity of Liquid Crystals to Cells	134
3.3.2	Effects of Cytochalasin-B, Trypsin and Ethanol to the Cells Adhesion on the Liquid Crystal Substrate.....	136
3.3.3	Structure of F-actin and Vinculin.....	139
3.3.4	Expressions of Integrin $\alpha 2$, $\alpha 3$, $\alpha 5$, $\beta 1$ and the Associated Extracellular Matrix Proteins	144
3.3.5	Interface Patterns of Cell Adhesion	150
3.4	Summary.....	152
4	QUANTIFICATION, MODELLING, MEASUREMENT AND MAPPING OF CELL TRACTION FORCES ON THE LIQUID CRYSTAL BASED CELL TRACTION FORCE TRANSDUCER	154
4.1	Introduction.....	155
4.2	Material and Methods.....	156
4.2.1	Quantification of Cell Traction Force (CTF).....	156
4.2.2	Implementation of a 3D Finite Element Model for Focal Adhesion-Liquid Crystal	159
4.2.3	Development of a Cell Traction Force Measurement and Mapping (CTFM) Software.....	162

4.2.4	Determining the Spatial Resolution of CTFM Software.....	167
4.2.5	Statistical Analysis.....	167
4.3	Results and Discussion.....	168
4.3.1	Cell Relaxation and Calculation of Cell Traction Force	168
4.3.2	Determining the Cell Force-Deformation Relationship of the Liquid Crystals.....	170
4.3.3	Comparison with Previous Cell Traction Force Measurement Techniques	172
4.3.4	Finite Element Simulations of Focal Adhesion-Liquid Crystal Model	174
4.3.5	The Cell Traction Force Measurement and Mapping Software	180
4.3.6	Spatial Resolution of the Cell Force Measurement and Mapping Software	187
4.3.7	Analysis of the Traction Force Distribution of Quiescent Keratinocytes.	190
4.3.8	A Study on the Traction Force Distribution of a Migrating Keratinocyte	193
4.3.9	Comparison with Previous Cell Force Sensors Developed for the Study of Cell Migration.....	201
4.3.10	Advantages of Liquid Crystal Based Cell Traction Force Transducer.....	202
4.4	Summary.....	204
5	EVALUATION OF LIQUID CRYSTAL BASED CELL TRACTION FORCE TRANSDUCER.	206
5.1	Introduction.....	207
5.2	Material and Methods.....	208
5.2.1	Treatment of Cells with Different Concentrations of TGF- β 1	208
5.2.2	Quantifying Contraction Responses of Cells to TGF- β 1.....	209
5.2.3	Statistical Analysis.....	209

5.3	Results and Discussion.....	210
5.3.1	Differential Traction Forces of Cells Treated with Various Doses of TGF- β 1	210
5.3.2	Reliability of the Liquid Crystal Based Cell Traction Force Transducer ...	217
5.4	Summary.....	220
6	GENERAL CONCLUSIONS, THESIS CONTRIBUTION AND FUTURE WORK.....	221
6.1	Conclusions.....	222
6.2	Thesis Contribution.....	229
6.3	Suggestions for Future Work.....	232
6.3.1	Physical Property Enhancement and Software Development	232
6.3.2	Cell Biological Applications	233
7	REFERENCES.....	234
8	APPENDIX A: MATLAB CODES FOR THE CTFM SOFTWARE	252

LIST OF FIGURES

Figure 1.1. (a) A schematic diagram of epidermis and dermis (Alberts et al., 2002). (b) A photomicrograph of histological section for an epidermis. (Source: courtesy of School of Life Sciences, University of Bradford).....	7
Figure 1.2. A schematic diagram of cellular adhesion.	9
Figure 1.3. Structure of basal lamina and connective tissue	13
Figure 1.4. The structure of actin cytoskeleton, focal adhesion complexes, integrin receptors, and adhesion proteins.....	15
Figure 1.5. Assembly of globular proteins into long chain of actin filaments in helical structure.....	16
Figure 1.6. The mechanism of actin filaments contraction in bi-directions.	18
Figure 1.7. Sarcomeric appearance of the actin filament (Peterson et al., 2004). (Scale bar: 2 μm)	18
Figure 1.8. A schematic showing the sub-components of the lamellipodia and filopodia: (a) tip of lamellipodium, (b) actin meshwork, (c) region of major disassembly, (d) tip of filopodium, (e) bundle, and (f) undegraded filament which contributes to the cytoplasmic network (Small et al., 2002).....	19
Figure 1.9. Activation of actin filaments by Rho, Rac and Cdc42.....	20
Figure 1.10. The intracellular signaling pathway of TGF- β	21
Figure 1.11. Seven experimental techniques used in probing mechanical response of a cell. (a) Atomic force microscopy (b) magnetic twisting cytometry, (c) micropipette aspiration, (d) optical trapping, (e) shear flow, (f) soft substrate stretching (Bao and Suresh, 2003) and quartz crystal (Marx et al., 2005).	23
Figure 1.12. Cells force sensor based on silicon rubber. Wrinkling patterns produced by (a) a chicken heart fibroblast (Harris et al., 1980). (Scale bar: 50 μm), and (b) fish Keratocyte on improved silicon rubber sheet (Burton et al., 1999). (Scale bar: 10 μm).....	25
Figure 1.13. The structure of a typical polymer with macromolecules that are cross-linked by covalent chemical bonds.....	26

Figure 1.14. Embedded marker based method. (a) A fish keratocyte cultured on the silicon sheet with embedded latex beads (Oliver and Pharr, 1992), and (b) a fibroblast migrating on the polyacrylamide (PAA) gel with fluorescence beads (Munevar et al., 2001). The arrows show the direction of the migration.....	28
Figure 1.15. Patterned PDMS and silicon nano wires used for measurements of cell traction force. (a) A mouse 3T3 (Tan et al., 2003), and (b) a Madin-Darby Canine Kidney (MDCK) epithelial cell shearing the micro-pillars of PDMS (Roure et al., 2005). (c) A mechanocyte bending silicon nanowires, and (d) a close up view of the cell-wire contacts (Li et al., 2009).....	29
Figure 1.16. Distortion created by a rat cardiac fibroblast on a micro-patterned silicon elastomer. (a) A cardiac fibroblast contracting on the surface of the elastomer substrate and (b) after relaxation with 2,3-butanedione monoxime (BDM). BDM is an inhibitor of the cytoskeleton (Balaban et al., 2001). (Scale bar: 10 μ m).....	30
Figure 1.17. G' and G'' of (a) cured PDMS and (b) PDMS solution published in (Lin et al., 2009) and (Ghannam and Esmail, 1998a) respectively.	33
Figure 1.18. A liquid crystal molecule of 5CB.....	35
Figure 1.19. A lyotropic liquid crystal molecule (Priestley et al., 1974).....	37
Figure 1.20. The typical phases of lyotropic liquid crystals. The figure illustrates the relationship between the amphiphile compositions at various temperatures producing a very dilute surfactant solution (W), aqueous surfactant solution (L_1), micellar cubic phase (I_1), hexagonal phase (H_1), bi-continuous cubic phase (V_1) and Lamellar phase (L_α). (Fairhurst et al., 1998)	38
Figure 1.21. Melting points of MBBA	40
Figure 1.22. Three main mesophases of liquid crystals	40
Figure 1.23. (a) Uniform and (b) Schlieren patterns of a nematic liquid crystal. (Scale bar: 50 μ m)	41
Figure 1.24. The orientation and distribution (order S) of mesogens.	42
Figure 1.25. A photomicrograph of Cholesteric 'oily-streaks' or Grandjean texture at room temperature. (Scale bar: 50 μ m).....	43
Figure 1.26. Smectic A phase of the smectic liquid crystals (Dierking, 2003).	44
Figure 1.27. Components of liquid crystal curvature. (a) Splay (b) Twist and (c) Bend (Frank, 1958).....	46

Figure 1.28. Process of developing a hybrid Liquid Crystal based Cell Traction.....	55
Figure 2.1. Chemical structure of the (a) cholesteryl chloride, (b) cholesteryl oleyl carbonate and (c) cholesteryl perlagonate.....	59
Figure 2.2. (a) The solid mixtures of cholesteryl ester liquid crystals in vials, (b) the mixtures melted at melting temperature (112 °C), and (c) Cholesteryl ester liquid crystals gel at room temperature (25 °C). Labels of P1, P2 and P2 on the vials represent CELCP1, CECLP2 and CELCP3, respectively.	59
Figure 2.3. (a) A Zeiss AxioPlan2 digital microscope, and (b) Thermal analysis under a DSC Q2000 system.	60
Figure 2.4. Liquid crystal substrates in the (a) absence (CELCP2) and (b) presence of RPMI-1640 cell culture media (LLC).....	61
Figure 2.5. Samples of CELCP2, LLC24hours, LLC48hours, and LLC72hours (a) before, and (b) after incubation in cell culture media for 24, 48 and 72 hours at 37 °C.	62
Figure 2.6. (a) A MCR501 rheometer and (b) LC sample under test.....	63
Figure 2.7. Deposition of cell suspension on a liquid crystal substrate before an addition of RPMI-1640 media.....	65
Figure 2.8. A bath of 2 % Formaldehyde in HBSS containing cell cultured on the liquid crystal substrate.....	66
Figure 2.9. (a) AFM nano-indentation of cholesteryl ester liquid crystal after incubation in cell culture media at 37 °C for 24 hours. (b) Schematic diagrams depicting the loading and unloading of an indenter and the associated displacement parameters. The parameter, r denotes the radius of a tip. 68	68
Figure 2.10. A typical load-displacement curve with the associated indentation depth and load parameters.....	69
Figure 2.11. (a) A steel ball of 500 μm diameter loaded to the liquid crystal surface in the cell culture media captured with a digital camera (Scale bar: 1 mm); Insert: The phase contrast image of a steel ball. (b) A schematic describing the spherical indentation to surface of the liquid crystal substrate in the cell culture media and the measurement parameters.....	71
Figure 2.12. Uni-axial tensile strain of a gel sample at (a) initial state and (b) after strain in traverse direction, x	74
Figure 2.13. A schematic diagram of a custom-built uni-axial micro-tensile stretch system.	75

Figure 2.14. (a) The actual setup of a micro-tensile system for measuring Poisson's ratio of cholesteryl ester liquid crystals, and (b) an image showing the temperature of a sample maintained at ~ 37 °C.	75
Figure 2.15. (a) Cross-polarising micrographs of nematic liquid crystals TL205 and CELCP1-P3 examined at (a-d) 20 °C and (e-h) 37 °C, respectively. (Scale bar: 50 μm)	80
Figure 2.16. (a) Cross-polarising micrographs of CELCP1-P3 sandwiched between a two cover slips examined at 20 °C. (b) CELCP1-P3 sandwiched between two cover slips. This image was taken with a black background. (Scale bar: 50 μm).....	80
Figure 2.17. DSC profiles for the three compositions of cholesteryl liquid crystals CELCP1, CELCP2 and CELCP3. No exothermic or endothermic activities were observed at 37 °C. T_g denotes glass transition temperature. T_m denotes melting temperature.	81
Figure 2.18. The texture of cholesteryl ester liquid crystals CELCP2. (Scale bar: 50 μm)	82
Figure 2.19. (a-b) Cross-polarised micrograph show a similar liquid crystal membrane drifting off the bulk cholesteric liquid crystal or the defective lyotropic liquid crystals. (c) A DIC and (d) a cross-polarised micrographs of the same defect-free liquid crystal film examined in isolation. (Scale bar: 25 μm). ..	83
Figure 2.20. A cross-polarising micrograph of cholesteric based lyotropic liquid crystals shows the wide band streaks and focal conic textures.	84
Figure 2.21. The proposed structure for the cholesteryl ester based lyotropic liquid crystals.	85
Figure 2.22. A schematic describing the effect of shear stress to the uni-axially aligned smectic lyotropic liquid crystals.....	85
Figure 2.23. Amplitude sweep data showing strain dependent storage modulus (G') and loss modulus (G'') at angular frequencies: (a) $\omega = 10 \text{ s}^{-1}$, (b) $\omega = 1 \text{ s}^{-1}$, and (c) $\omega = 0.1 \text{ s}^{-1}$ for LLC24hours, LLC48hours and LLC72hours, respectively.....	87
Figure 2.24. Stress-strain curves of CELCP2, LLC24hours, LLC48hours and LLC72hours from 0.1 % up to a strain of (a) 100 % and (b) 10 % at $\omega = 0.1 \text{ s}^{-1}$. The linear regression lines were used to approximate the linear viscoelastic range of the liquid crystals.....	90
Figure 2.25. Simple shear of the liquid crystals. Left: Top view, Right: Cross-section. .	91

- Figure 2.26. The frequency sweep results. (a) Shear rate dependent storage modulus (G' , square), loss modulus (G'' , triangle) and complex viscosity (η^* , circle) of the CELCP2 (Yellow), LLC24hours (Green), LLC48hours (Red) and LLC72hours (Blue) obtained for angular frequencies from 0.01 s^{-1} to 100 s^{-1} at 5 % strain. (b) The bar charges of storage and loss moduli obtained at $\omega = 0.01 \text{ s}^{-1}$. The scatter plot shows the complex viscosity (η^*) of CELCP2, LLC24hours, LLC48hours and LLC72hours. The asterisks (*) indicate that the storage modulus, loss modulus and complex viscosity for LLC72hours are significantly different from the CELCP2 (significant for $p < 0.05$, Tukey HSD test, $N = 3$). 93
- Figure 2.27. (a-d) Phase contrast micrographs of the cells cultured on the liquid crystal substrates, and (e-f) cells adhering to a membrane drifting off the bulk liquid crystals. Enlarge exert of (a) shows the short deformation lines radiating out of the periphery of a cell. (Scale bar: $20 \mu\text{m}$) 98
- Figure 2.28. HaCaT cells cultured on LC surface in response to $30 \mu\text{M}$ cytochalasin-B treatment and direction of LC deformation lines shrinkage at (a) 0 minute, (b) 30 minutes, and (c) 60 minutes. Solid line arrows show the direction of the cell contraction and relaxation after treated with cytochalasin-B. Dotted line arrows show the repelling directions of the deformation line. (d) A depiction showing the correlation of the deformation line formed on the liquid crystal film with transverse shear forces induced by the contractions of cell circumferential actin filaments that are anchored at the focal adhesions. Treatment with cytochalasin-B caused F-actin depolymerisation, force degeneration and diminishing deformation lines of the liquid crystal surface. (Scale bar: $25\mu\text{m}$) 99
- Figure 2.29. (a) Phase contrast and (b) cross-polarising micrographs of deformation lines induced by HaCaT cells in the LC surface. The profile plots for the cross-section of a deformation line as shown and marked in (a) and (b). (Scale bar: $25 \mu\text{m}$) 100
- Figure 2.30. Phase contrast micrographs showing the effect of $30 \mu\text{M}$ cytochalasin B on HaCaT cells cultured over the lyotropic liquid crystals after 24, 48 and 72 hours of incubation taken every 5 minutes over a period of 60 minutes. The time shown is the period of treatment of cells in cytochalasin-B. (Scale bar: $25 \mu\text{m}$) 103
- Figure 2.31. (a) Time series images taken every 24 hours up to 96 hours for HaCaT cells treated in 2 % formaldehyde. The arrows in (a) show the deformation lines that were monitored for their changes of length; (b) Length of deformation lines measured (mean \pm SD, $N = 28$, 3 repeats) after cells treated in formaldehyde for 24, 48, 72 and 96 hours. The arrows show the example of deformation lines used for quantification. (Scale bar: $25\mu\text{m}$) 105
- Figure 2.32. A load-displacement curve of the liquid crystals surface and the relations to the loading and unloading of an indenter. 108

- Figure 2.33. (a) Cross-polarised micrographs show the elastic recovery of deformed liquid crystals (0 - 15 seconds) after a steel ball was being unloaded. The inset shows the steel ball with a diameter of 500 μm before unloading. (Scale bar: 50 μm) (b) A graph of vertical displacement (δ) versus loading time for $N = 3$ shows the creep deformation of the liquid crystals..... 110
- Figure 2.34. Phase contrast micrographs show the behaviors of the lyotropic liquid crystals after a steel ball was unloaded. They were incubated at 37 $^{\circ}\text{C}$ for (a) 24, (b) 48 and 72 hours, respectively 113
- Figure 2.35. (a) Uni-axial deformation of a solid PDMS. The bi-headed arrows show the deformation in longitudinal direction (y) of PDMS at 380 μm , 276 μm , 220 μm , 192 μm and 178 μm that are corresponding to the deformation in transverse direction (x) at 10, 20, 30, 40 and 50 μm , respectively (image from left to right). The first image from the left shows the measurement for x_0 and y_0 . (Scale bar: 50 μm) (b) Plots of logarithmic longitudinal strain (ϵ_2) versus transverse strain (ϵ_1) or the Poisson's ratio of PDMS at room temperature (25 $^{\circ}\text{C}$) in three repeat of experiments ($N = 10$ per experiment). 116
- Figure 2.36. Uni-axial deformation of CELC. The bi-headed arrows show deformation in longitudinal direction (y) of LLC at 490 μm , 260 μm , 190 μm and 90 μm that are corresponding to the transverse deformation (x) at 50, 100, 150 and 200 μm , respectively (image from left to right). The first image from the left shows the measurement for x_0 and y_0 . (Scale bar: 200 μm) 117
- Figure 2.37. Plots of logarithmic longitudinal strain (ϵ_2) versus transverse strain (ϵ_1) or the Poisson's ratios for CELC and LLC up to (a) $\log \epsilon_1 = 0.2$ (60 % of strain) and (b) $\log \epsilon_1 = 0.8$ (600 % of strain) determined at 25 $^{\circ}\text{C}$. The data are expressed as means \pm SD. 118
- Figure 2.38. (a) Plots of logarithmic longitudinal strain (ϵ_2) versus transverse strain (ϵ_1) or CELC and LLC incubated at 37 $^{\circ}\text{C}$ for 24, 48 and 72 hours. The data are expressed as means \pm SD. (b) A comparison of Poisson's ratio (mean \pm SD) for CELC and LLC at room (25 $^{\circ}\text{C}$) and incubation temperature (37 $^{\circ}\text{C}$). . 119
- Figure 3.1. Preparation of liquid crystal samples in 15 wells (left, middle). Cell suspensions cultured in the presence of four liquid crystals (CELCP1, CELCP2, CELCP3 and TL205) and controls in 15 well cultures (right). 125
- Figure 3.2. A cell relaxation technique implemented by applying Cytochalasin-B and trypsin to cells cultured on liquid crystal substrates (LCS) in petri dishes. Ethanol was used as a control. 126
- Figure 3.3. A Nikon Eclipse 80i immunofluorescence microscope system. 131
- Figure 3.4. Cell culture in the absence (left) and presence (right) of liquid crystals on gold substrate. 132

Figure 3.5. (a) A Wide Field Surface Plasmon microscope and (b) the setup for imaging fixed cells. The red circle in the image shows the location of the gold substrate holder and the oil immersion lens in the setup.	133
Figure 3.6. HaCaT cells cultured on (a) CELCP1, (b) CELCP2, (c) CELCP3, and (d) TL205 at a cell density of approximately 1200 cells/cm ² (Scale bar: 25 μm)....	135
Figure 3.7. Percentage of HaCaT cell viability (mean ± SE) in cholesteric and nematic liquid crystals relative to control.	136
Figure 3.8. Phase contrast micrographs for the treatment effects of (a) 0.0042 % (v/v) ethanol (control), (b) 30 μM cytochalasin B, and (c) 0.25 % trypsin to the cells taken every 5 minutes over a period of 60 minutes. The area of cell attachment in μm ² are as outlined in the micrographs. (Scale bar: 25 μm)	137
Figure 3.9. Phase contrast micrographs show the interface of HaCaT cells attached to (a) a plain glass and (b) a liquid crystal substrates. Immunofluorescence micrographs of the staining against (c, d) F-actin, and (e, f) vinculin, respectively. (Scale bar: 25 μm) (Enlarge exert, scale bar: 1 μm)	141
Figure 3.10. A comparison of (a) vinculin width (p = 0.383), length (p = 0), and (b) cell surface area (p = 0) of HaCaT cells attached to plain glass cover slips and liquid crystal substrates. The area of cells, length and width of vinculin are expressed as mean ± standard error which is significant for P < 0.001, N = 258 (cell surface area) and N = 525 (vinculin).	142
Figure 3.11. Micrographs of immunocytochemical staining against α2, α3, α5 and β1 for (a, d, g, j) negative controls, HaCaT cells cultured on (b, e, h, k) glass cover slips and (c, f, i, l) liquid crystal substrates, respectively. (Scale bar: 25 μm).....	145
Figure 3.12. Micrographs of immuno-staining against collagen type IV, laminin and fibronectin for (a, d, g) negative controls, HaCaT cells cultured on (b, e, f), controls and (c, f, i) liquid crystal substrates, respectively. (Scale bar: 20 μm). (Enlarged exert, scale bar: 25 μm).	146
Figure 3.13. Immunoperoxidase staining of laminin for HaCaT cells cultured on a negative control (left), control (middle) and liquid crystal substrate (right).	147
Figure 3.14. A propose model for the interaction of cell membrane and cholesteryl ester based lyotropic liquid crystals.	149
Figure 3.15. WSPR micrographs show the patterns of cells adhesion on the (a) hard cover slip, (b) soft liquid crystals and (c-d) their associated 3D structures displayed in ImageJ software, respectively. (Scale bar: 10 μm).....	152

Figure 4.1. (a) Schematic diagram showing lateral view of a cell inducing deformations in the liquid crystal surface due to the contractions of circumferential actin filaments exerting traction force via the focal adhesions. (b) The dimensions of a stress site in LC surface which was loaded (dotted line) and unloaded (solid line) by compressive force (F) applied to the focal adhesion area or stress plane (A). 157

Figure 4.2. (a) Parametrical geometry of the focal adhesion-liquid crystal model. L_{fa} , H_{fa} , W_{fa} , L_{lc} , H_{lc} , and W_{lc} are the length, height and width of the focal adhesion (denoted as fa) and the liquid crystal substrate (denoted as lc), respectively. (b) Schematic diagram of a stress site in the LC surface which is under uni-axial compressive force (F) loaded by two clusters of focal adhesion to the two stress planes. Bottom: the associated tensor diagram in three dimensions. The plane stresses, σ_{xx} cause shear stress of τ_{xz} and τ_{xy} in the y and z directions. 160

Figure 4.3. Flow chart of the cell traction force measurement algorithm 164

Figure 4.4. Flow chart of the cell traction force mapping and rendering algorithm. . 166

Figure 4.5. (a) The treatment effects of 30 μ M cytochalasin-B in phase contrast micrographs taken at 0 and 30 minutes for a cell cultured on the surface of the liquid crystals. (Scale bar: 10 μ m) (b) Enlarge exerts for the deformation lines are as shown and labelled in the boxes of (a). The inward and outward arrows show the directions of force application and degeneration, respectively. (Scale bar: 5 μ m)..... 169

Figure 4.6. (a) The relationship of longitudinal deformation length (y_o) to the transverse displacement. (b) The relationship of traction force (F) to the transverse displacement (Δx). (c) The relationship of traction force (F) to the longitudinal deformation (y_o). The traction force was calculated for ten non-motile keratinocytes (N = 55). 171

Figure 4.7. Normally distributed traction forces ($p = 0.187$, significant for $p > 0.05$) for ten non-motile keratinocytes. N = number of deformation line..... 173

Figure 4.8. A mesh containing 10842 triangular elements at a size of 5.7 μ m was used in generating the solid mesh for the focal adhesion-liquid crystal model. 175

Figure 4.9. (a) Transverse displacement and stress plotted simulated by Finite Element analysis for the keratinocyte in Figure 4.5. 176

Figure 4.10 The calculation and simulation for the (a) compressive force versus transverse displacement, and (b) stress versus transverse displacement for the cell in Figure 4.5. 177

Figure 4.11. (a) A 3-D topography of a deformation with displacements in the liquid crystals induced by the loads via the contact planes. Inset: The dimensions of the focal adhesions used in the finite element model. (b) Von-mises stresses computed for the compressive loads.	178
Figure 4.12. The distribution of stresses and transverse displacements across a deformation site.	179
Figure 4.13. The GUI of the cell force measurement and mapping software.	180
Figure 4.14. Defining the start and points for calibrating the scale of the image.	181
Figure 4.15. Entering the image scale (20 μm) in the pop-up window.....	181
Figure 4.16. Use of mouse to define a deformation line and displays of the calculated force values.....	183
Figure 4.17. The display of traction forces and the average traction force of a cell...	183
Figure 4.18. A display of force data points (z) over the x and y Euclidean coordinate system.	184
Figure 4.19. The fitting of force data curves by using (a) linear and (b) cubic interpolations.....	185
Figure 4.20. 2D cell traction force maps which were fitted with (a) linear and (b) cubic interpolations.....	186
Figure 4.21. Spatial resolution of a liquid crystal based cell traction force transducer. (Enlarged exert, scale bar: 5 μm).....	187
Figure 4.22. Phase contrast micrographs of PDMS calibration gauges consisting of line patterns with an interval of (a) 3 μm and (b) 5 μm	188
Figure 4.23. The resolution of CTFM software in resolving forces separated by a distance of (a) 3 μm and (b) 5 μm . x and y are the Euclidean coordinates and z is the axis for the traction force in the unit of nano-Newton. The scale bar in pseudo colours represents the magnitude of forces.	189
Figure 4.24. (a) A single HaCaT cell contracting on the LC traction force transducer and (b) the force distribution rendered by CTFM system. The arrows indicate the region of protrusion.	190
Figure 4.25. (a) Two adjacent HaCaT cells contracting on the LC force transducer, and (b) the force distribution generated by CTFM software.	191
Figure 4.26. (a) A polarised HaCaT contracting on the LC traction force transducer, and (b) the force distribution generated by CTFM software.	191

- Figure 4.27. Time base tractions of a keratinocyte on a LCTFT shown in (a) phase contrast micrographs taken at 0, 5, 10 and 15 minutes of monitoring. The broken line arrow indicates the direction of movement and the dotted lines are the position of reference for the cell. (b) The associated distribution of traction forces. (c) The directions of forces as shown with thick arrows and the thin arrows represent the direction of the actin bundles, respectively. The scale bar in pseudo color represents the magnitude of forces. (Scale bar: 20 μm) 195
- Figure 4.28. Time response curves of the traction force measured at different regions of a single keratinocyte as shown in Figure 4.27..... 196
- Figure 4.29. (a) Circumferential actin filaments and (b) vinculins located at the lamella of the keratinocytes cultured on LC substrate. The arrow heads indicate the short actin bundles and focal adhesions located at the circumference of the keratinocytes in (a) and (b), respectively. (Scale bar: 25 μm) 198
- Figure 4.30. A new model proposed for the contraction of circumferential and straight actin bundles of a migrating keratinocyte in relation to the deformation lines form in the liquid crystals..... 198
- Figure 5.1. Phase contrast micrographs of HaCaT cells contracting on the surface of the liquid crystals in (a) a control and in the treatments with single dose TGF- β 1 at (b) 5 ng/ml, (c) 10 ng/ml, and 20 ng/ml at 37 $^{\circ}\text{C}$ for 24 hours. (Scale bar: 20 μm) 211
- Figure 5.2. Average traction forces (mean \pm SE) of HaCaT cells in a control (0 ng/ml) and after treated with of single dose TGF- β 1 at 5 ng/ml, 10 ng/ml and 20 ng/ml at 37 $^{\circ}\text{C}$ for 24 hours in three repeats of experiments (N = 100 cells per experiment)..... 212
- Figure 5.3 The distribution of traction forces for HaCaT cells in the (a) control and after treated with different concentrations of single dose TGF- β 1 at (b) 5 ng/ml, (c) 10 ng/ml, and 20 ng/ml for 24 hours at 37 $^{\circ}\text{C}$ in three repeats of experiment (N = 100 per experiment)..... 213
- Figure 5.4. Percentage (Mean \pm SD) of HaCaT cells responded in contractions to various concentration of single dose exogenous TGF- β 1 at 37 $^{\circ}\text{C}$ in three repeats of experiment (N = 100 cells per experiment)..... 215
- Figure 5.5. Traction forces (means \pm SE) of HaCaT cells cultured on three isolated liquid crystal substrates (LCS) that were treated with TGF- β 1 at 0, 5, 10 and 20 ng/ml in three repeats of experiment (N = 100 cells per experiment), respectively. Mann-Whitney post hoc tests indicate that the treatments between 0 and 5 ng/ml ($p = 0$), 5 and 10 ng/ml ($p = 0$), 10 and 20 ng/ml ($p = 0.008$) are significantly different for $p < 0.05$ in One-way ANOVA analysis. The asterisk * indicates that there is a significant difference in between treatments. 219

LIST OF TABLES

Table 1.1. Associated ligands receptor identified for human keratinocytes migration.	16
Table 1.2. Comparison of cell force measurement techniques	31
Table 1.3. Applications of the liquid crystals as biosensors.....	48
Table 2.1. Shear Sensitive Liquid Crystals in different formulations.	58
Table 2.2. Test of normality for storage modulus and loss modulus of the CELCP2 which is significant for $p > 0.05$. Each sample of CELCP2 was tested 3 times.	92
Table 2.3. Comparison of Young's modulus of cholesteryl ester based lyotropic liquid crystals (after 24 hours of incubation) determine by using AFM based nano-indentation and spherical indentation.....	111
Table 4.1. Properties of liquid crystals and dimension of vinculin	160
Table 4.2. Comparison of other epithelial cell force measurement techniques	174
Table 5.1. Mean ranks for traction forces of HaCaT cells treated with HBSS (control) and with different doses of TGF- β 1 obtained from Kruskal-wallis test. N represents the number of cells.	218

CHAPTER 1

INTRODUCTION

“This journey of a thousand miles begins with a single step”-Lao Tzu

1.1 Research Background

Pharmacology is an experimental science which involves studying the effects of chemically active molecules on physiological activity. As one of the cornerstones in new drug development, pharmacology investigates the effects of new drugs through screening for desired activity, determining the mode of actions and defining the drug therapeutic function. Pharmacological studies involving animals in biological assays started as early as the 19th century (Fastier and Reid, 1949). Mammals such as rats, guinea pigs, rabbits and dogs are the most commonly used experimental subjects. In pre-clinical testing, organs or tissues are excised surgically and prepared for pharmacological study in oxygenated physiological solution within an organ bath. The organ bath technique was first applied by Henrick Magnus in 1904 on a strip of small intestine (Fastier and Reid, 1949). Today, the organ bath is still being used extensively to investigate the physiology and pharmacology of various tissues such as muscle, arterial rings, uterine tissue, ileum, colon arterial and diaphragm. In an organ bath, a section of tissue is suspended between a fixed point and an isotonic or isometric force transducer in a pre-warmed Krebs solution (Bennett and Pettigrew, 1974). Rhythmic contraction and relaxation of the tissue creates variable load forces which the force transducer converts into electrical signals (Bennett and Pettigrew, 1974). In modern systems, the electrical signals are digitised and displayed on a computer monitor as traces of contractility. Stimulation of the tissue can be induced by chemical, electrical or physical means. The range of sensitivity in terms of force transduction of commercial systems is from 50 μ N to 250 mN (ADINSTRUMENT Incorporation and DMT Incorporation).

New developments in the agricultural and pharmaceutical industries require stringent evaluation and assessment of compounds before clinical trials. Prudent pre-

clinical trials usually involve large numbers of rodent and non-rodent mammalian species (Ganter et al., 2005, Jacobson-Kram and Mills, 2008). Recently, the United States Food and Drug Administration (FDA) issued a guide on Exploratory Investigational New Drug (IND) to reduce animal exploitation and simultaneously to accelerate the development of new pharmaceutical agents (Jacobson-Kram and Mills, 2008). Similarly, a new directive concerning cosmetic products (2000/0077(COD)) aims at reducing animal testing by promoting the design of in-vitro toxicological assays. Thus, cell line based culture assays are attracting interest as an alternative for drug and cosmetic testing. However, to enable this highly sensitive and high throughput screening, accurate analytical techniques for sensing cellular activities are required. During pre-clinical testing, application of an agonist and an antagonist to a tissue in an organ bath induces contraction and relaxation of a tissue, which is measured in terms of force. The question is how did the drug trigger the action of the tissue? This analysis in a tissue constructed from many different cells types is difficult (for example, the same section of tissue may contain neurons, smooth muscle cells and fibroblasts), thus, the characterisation of cell physiological responses may provide more insights if determined by examining the contractile properties of the individual cells (Bitar and Makhoul, 1985, Li et al., 2009, Ma et al., 2002).

Motivated by the need to assess single cell contraction induced by chemical stimuli, contractility assays measuring the change in average cell length of a large population of smooth muscle cells were developed to study the responses of smooth muscle to agonists such as endothelin-1, interleukin, C-terminal octapeptide of cholecystinin, acetylcholine and methoionine-enkephalin (Bitar and Makhoul, 1985, Moumni and Woodford, 1992, Dallot et al., 2003, Akiho et al., 2002). These studies identified a number of advantages of single cell based biological assays for the

pharmaceutical industry such as: (a) the easy characterisation of surface receptors as a consequent of drug action, and (b) highly repeatable screening (Dallot et al., 2003, Akiho et al., 2002).

Thereafter, many single cell based biosensors have been developed for use in pharmacological screening (Stenger et al., 2001, Park and Shuler, 2003). In a cell based biosensor system, the cell is the primary detector which converts the molecular signals into electrophysiological or mechanical signals; these signals are then transduced by a secondary transducer in the form of electrode, magnetic or optical detector. Overall, the techniques in measuring physiological responses of single living cells to analytes can be classified into two broad categories: electrophysiology and mechanobiological measurement systems. Each category has its own advantages and disadvantages.

Electrophysiological techniques originated from neuroscience, in which, systems were developed to study the electrical activity of nerves cells (Hodgkin and Keynes, 1955, Hodgkin, 1937, Gross et al., 1972). These systems have since been employed to study other electrogenic cells such as smooth muscle and cardiac myocytes (Thomas, 1972, Hara et al., 1986, Cranefield and Hoffman, 1958). These techniques involve the use of electrodes to sense the depolarisation or hyperpolarisation of action potential of cells attaching to the electrodes (Gross et al., 1972). Patch clamp (Kraft and Patt, 2006, Betz. W. J. and Sakmann, 1971), potassium chloride filled glass electrode (Dole, 1941) and planar patch clamp (Behrends and Fertig, 2007) technique are among the classical electrophysiology techniques developed to monitor the activities of individual ionic channels in the cell membrane. In these systems, the recording can be intracellular or extracellular in a cell culture. Unfortunately, these techniques are time consuming and because of their invasive nature, they often result in cell death. One of the alternatives is monitoring cell electrophysiology using micro-fabricated

extracellular electrode recording or microelectrode array systems (Kovacs, 2003, Fromherz, 2003). These systems rely on culturing electrogenic cells over miniaturised recording sites made of gold or indium-tin-oxide, or arrays of field effect transistor electrodes to monitor signals from those cells directly positioned over the recording sites (Fromherz, 2003, Kovacs, 2003, Thomas et al., 1972, Gross et al., 1977, Offenhausser et al., 1997). These systems have been used to generate dose response curves for known pharmacological agents (Yu et al., 2006) but are subject to limitations associated with sensitivity and reliability (Muthuswamy et al., 2005, Shoham et al., 2006)

In the measurement systems using microelectrode, the electrodes allow recording of electrical activity at single point of the cell membrane or tissue but this does not provide information about the spatial distribution of bioelectric activity over the cell membrane (Loew, 1996). To circumvent this issue, an optical electrophysiology technique has been developed which involves the use of potential-sensitive dyes or fluorescing proteins that are capable of changing the fluorescence intensity when these probes detected sub-millisecond membrane potential changes or intrinsic birefringence (Obaid et al., 2004, Cohen and Salzeberg, 1978, Loew, 1996). The potential-dependent characteristic is able to shift the excitation spectra, and thus allowing the quantification of membrane potential (Waggoner, 1979, Cohen and Salzeberg, 1978). After the tissue or cell is perfused or injected with the potential sensitive dye, two-dimensional (2D) distribution of colour intensity along the cell membrane corresponding to the field potential can be visualised and recorded. Some dyes developed earlier such as cyanine dyes are believed to inhibit the metabolic activity or inducing photodynamic damage due to the strong illumination of these dyes (Waggoner, 1979, Obaid et al., 2004). Therefore, the potentiometric dyes developed later (Potential-sensitive ANEP dyes, Invitrogen) aim to overcome these problems.

These dyes improved the signal to noise ratio and reducing dye internalisation (absorption into the nucleus). However, these dyes still needed to be solubilised in dimethyl sulfoxide (DMSO) and are limited by moderate phototoxicity (Obaid et al., 2004). Phototoxicity increases oxygen radicals in cell cultures and can be cytotoxic in the long term (Obaid et al., 2004).

Electrophysiological measurements are more suitable for electrogenic cells that fire large action potentials. Monitoring the physiological changes of epithelial cells is more related to the measurement of cell mechanical activity in terms of forces (for example, contraction or traction forces). Traction forces are defined as forces that a cell exerts tangentially on a substrate (Oliver et al., 1998). They are the indications of the contractile forces generated within the cell cytoskeletons. Studies on how the contraction forces are generated and transmitted by a single cell as traction forces to the adjacent cell and extracellular matrix (ECM) set the foundation for the development of cell traction force (CTF) measurement technique.

1.2 Cellular Adhesion, Contraction and the Measurements of Cell Traction Force

1.2.1 Epidermal Tissue

The skin is made up of three major layers, the epidermis, dermis and hypodermis (Gawkrodger, 2003). The epidermis forms the outermost layer of skin and is constructed from four layers known as the basal, spinous, granular and cornified layer (Figure 1.1). The epidermis protects the underlying tissues of skin from abrasion and contains four major cell types (keratinocytes, melanocytes, langerhans cells and

merkel cells) (Gawkrodger, 2003). Of these cells, the keratinocytes make up about 90 % of the epidermis (Rocchad and Barrodon, 2009).

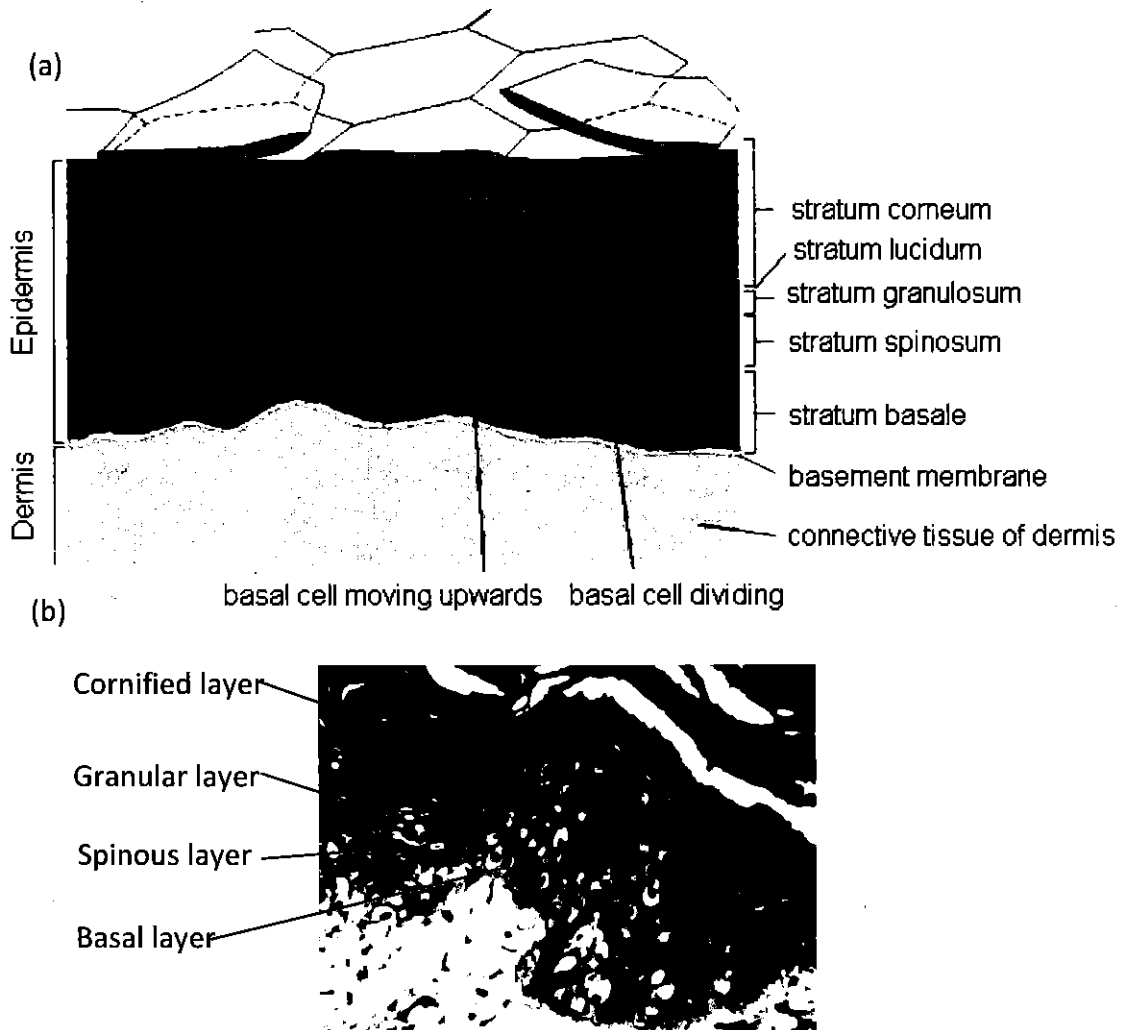


Figure 1.1. (a) A schematic diagram of epidermis and dermis (Alberts et al., 2002). (b) A photomicrograph of histological section for an epidermis. (Source: courtesy of School of Life Sciences, University of Bradford).

By division of keratinocyte stem cells at the basal layer, new epidermal cells (keratinocytes) are formed at the spinous layer (stratum spinosum) and further division continues to form the granular layer (stratum granulosum) (Hendriks, 2005). The presence of lipids in the stratum granulosum creates a hydrophobic barrier between the stratum granulosum and the stratum lucidum that prevents dehydration (Feingold, 2007). As the keratinocytes translocate superficially, the cells increase their

keratin content to protect the skin and underlying tissue from environmental damage such as ultra violet light and dehydration. Newly produced keratinocytes gradually differentiate and move upwards to replenish the overlying cells of the stratum lucidum (Gawkrodger, 2003). This process of terminal differentiation and migration continues until the cells die and become enucleated cells in the protective stratum corneum or cornified layer (Feingold, 2007).

Even though protected by the stratum corneum, the skin is delicate and can be wounded when being exposed to abrasion of sharp objects. However, under small levels of compression or shear on the skin surface, the tissue is elastic and can return to its original state upon release of applied stress. The elasticity and integrity of the skin is due to the structural organisation and strong traction forces between cells, and also, between cells and the extracellular matrix (Silver et al., 2003).

1.2.2 Cellular Adhesion

The contact which leads to the binding of a cell to a surface, another cell or the extracellular matrix is known as cellular adhesion (Dzamba et al., 2001). Cell adhesion is mediated by cell junctions (Vasioukhin et al., 2000). Cell junctions are divided into two broad classes, the intercellular junctions and the extracellular junctions. Intercellular junctions (Figure 1.2) are those that link cells to other cells such as the tight, gap, adherens and desmosomal junctions (Vasioukhin et al., 2000, Farquhar and Palade, 1963). Multiple adhesion molecules (for example, hemidesmosome and focal adhesions) are found in extracellular junctions and they function to attach cells to the extracellular matrix (ECM) (Farquhar and Palade, 1963).

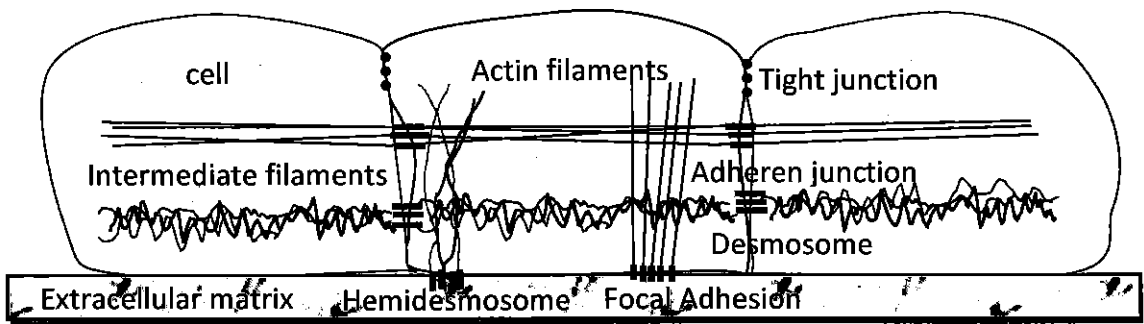


Figure 1.2. A schematic diagram of cellular adhesion.

Tight junctions (Figure 1.2) are formed from membrane proteins such as the claudins, occludins and e-cadherin that strongly couple the adjacent cell membranes (Schneeberger and Lynch, 1992, Furuse et al., 1998, Farquhar and Palade, 1963). As their names implies, molecules cannot pass through the sealed junctions, thus, allowing them to form a selective barrier. For example, it is this selective barrier in the endothelial cells that gives rise to the blood brain barrier (Wolburg et al., 1994).

Gap junctions are formed from membrane spanning proteins called the connexions. Gap junctions are continuous channels between two plasma membranes. These channels allow intercellular cytoplasmic communication and provide for cell-to-cell diffusion of small molecules, including ions, amino acids, nucleotides, and second messengers (Lampea and Laub, 2004). Gap junctions allow the propagations of action potential between cells (Rohr, 2004). Each gap junctions consists of 6 connexins subunits. These subunits are associated with the connexins of a neighbouring cell membrane, thus, forming channels that passes through the membrane of both cells (Lampea and Laub, 2004). Gap junctions are like valves and can be controlled locally. They are found between cardiac myocytes and smooth muscle cells that enable a coordinated contraction mediated by direct cell-cell impulse transmission (Lampea and Laub, 2004, Rohr, 2004).

Desmosome and hemidesmosome (Figure 1.2) are directly connected to the intermediate filaments at the extracellular junctions (Vasioukhin et al., 2000). Desmosomes link the intermediate filaments of a cell to the adjacent cell via calcium-dependent adhesion molecules or specialised cadherins called desmogleins and desmocollins (Gumbiner, 1996, Farquhar and Palade, 1963, Vasioukhin et al., 2000). Desmosomes are patch like junctions that are randomly distributed and fill the 30 nm gap between the attachment membranes (Green and Jones, 1996). Hemidesmosomes have a different function which is to connect the intermediate filaments of a cell to the ECM (Dzamba et al., 2001). They can be found in muscle cells or in stratified epithelial cells.

As shown in Figure 1.2, two extracellular junctions that are closely associated with the actin cytoskeleton are the adherens junctions and focal adhesions (Farquhar and Palade, 1963). Adherens junctions or Zonula adherens are complex proteins found at the sites of cell-cell adhesion (Farquhar and Palade, 1963). At the adherens junctions, the calcium dependent transmembrane proteins (E-cadherin) mediate cell to cell attachment (Vasioukhin et al., 2000). E-cadherins binds β -catenin which in turn binds α -catenin that link the actin cytoskeleton to the adherens junctions (Krendel et al., 1999). Focal adhesions are large macromolecules, comprise of a sub-membrane plaque which is made up of at least 50 different proteins and they mechanically bind the cell membrane to the ECM via specific transmembrane receptors (Matthews et al., 2006). Both the adherens junctions and focal adhesions connect to the actin filaments of the cytoskeleton and it is these actin filaments that exert traction forces on neighbouring cells and ECM (Burrige et al., 1986, Geiger and Ginsber, 1991).

In the epidermal layer, the ECM forms a complex meshwork which is produced and secreted by cells into their surrounding medium (filling between cells) (Buck and

Horwitz, 1987). In the connective tissue, fibroblasts mainly produce macromolecules in the ECM matrix. These macromolecules are formed from heavily glycosylated proteins giving rise to hydrogel like materials (such as, glycosaminoglycan (GAG) and proteoglycans) which contain various fibrous proteins (O'Toole, 2001). Fibrous proteins embedded in the polysaccharides gel (Hay, 1981) are made up of two functional groups, the structural (collagen and elastin) and adhesive proteins (fibronectin and laminin) (O'Toole, 2001, Gray et al., 2000). Structural proteins help to organise the matrix and provide resilience (Hay, 1981, Hook et al., 1984). For example, the GAG and proteoglycan gels withstand compressive forces or tension applied to the ECM while allowing the diffusion of nutrients and hormones between the blood and the cells (Hook et al., 1984). The adhesive proteins including collagen facilitate cell attachment to the ECM (Geiger et al., 2001). For example, laminin is associated with the attachment of epithelial cells to basal lamina, and fibronectin enables the attachment of fibroblasts and mast cells in the connective tissue (Kirfel and Herzog, 2004, O'Toole, 2001).

In the connective tissue of the dermis (Figure 1.3), collagen is the most abundant fibrous protein. This protein is characterised by long, stiff and triple-stranded helical structure of three single-polypeptide chains (or α chain) (Rich and Crick, 1955, Rest and Garrone, 1991). The single α -chain is constructed from many proline and glycine molecules (amino acids) (Rich and Crick, 1955, Rest and Garrone, 1991). About 28 types of α -chain molecules have been identified, including type I, II, III, V and XI collagen (Rest and Garrone, 1991, Heino, 2007). Type I is the principal collagen molecules that constituted the collagen fibres in tissue (Rest and Garrone, 1991). Type IV collagen molecules are network-forming collagen fibres that made up the meshwork

of the basal lamina, while type VII collagen binds the basal lamina to the underlying connective tissue (Heino, 2007).

Elastin is another structural protein and like collagen fibres are embedded in the ECM of skin, blood vessels and lungs (Hay, 1981). The network of elastin fibres exhibit elastic behaviour and they give tissues their elastic properties (Gotte and Serafini-Fracassini, 1963). The collagen fibrils are interwoven with the elastin fibres in order to prevent the tissue from over-stretching and tearing (Cleary and Gibson, 1983). The collagen fibres provide tensile strength while elastin fibres support tissue elasticity (Rosenbloom et al., 1993, Hay, 1981).

Fibronectin is an adhesive fibrous protein found in the connective tissue. This protein is a dimer composed of two very large subunits connected by disulfide bonds near the carboxyl terminal (Hynes and Yamada, 1982). Each subunit in the dimer has repeated sequences of what are referred to as type III fibronectin repeats (Hynes and Yamada, 1982). Along the repeating unit, there are binding sites for the heparin, collagen and specific transmembrane receptors found on the surface of the cells membrane (Hynes and Yamada, 1982). Some studies suggest that isoforms of fibronectin produced during wound healing specifically help in guiding cell migration and proliferations for new tissue development (Singer et al., 1999, Bartkova et al., 2003). Therefore, the adhesive function of fibronectin in attaching cells needs to be balanced with the needs of cell migration during wound healing (Larjava et al., 1993).

The basal lamina or basement membrane is formed from ECM proteins and it is especially rich in adhesion proteins (collagen, fibronectin and laminin) that are organised as a thin sheet underlying the epithelial cells. Hence, the basement membrane separates the cells from the connective tissue (Lillie et al., 1988, Larjava et al., 1993). In the epidermis, the basal lamina produced by the epithelial cells is divided

into two layers: lamina lucida overlying the lamina densa (Figure 1.3) (Laurie et al., 1982, Stanley et al., 1982b). The lamina lucida forms a boundary with the epithelial cells overlying the lamina densa (Laurie et al., 1982), whilst the lamina densa is connected to the underlying connective tissue by collagen fibrils (mainly made of type VII collagen molecules) (Laurie et al., 1982, Stanley et al., 1982b). The basal lamina containing the adhesion proteins can influence cells polarity, regulate cell metabolism and induce cells differentiation (Stanley et al., 1982b).

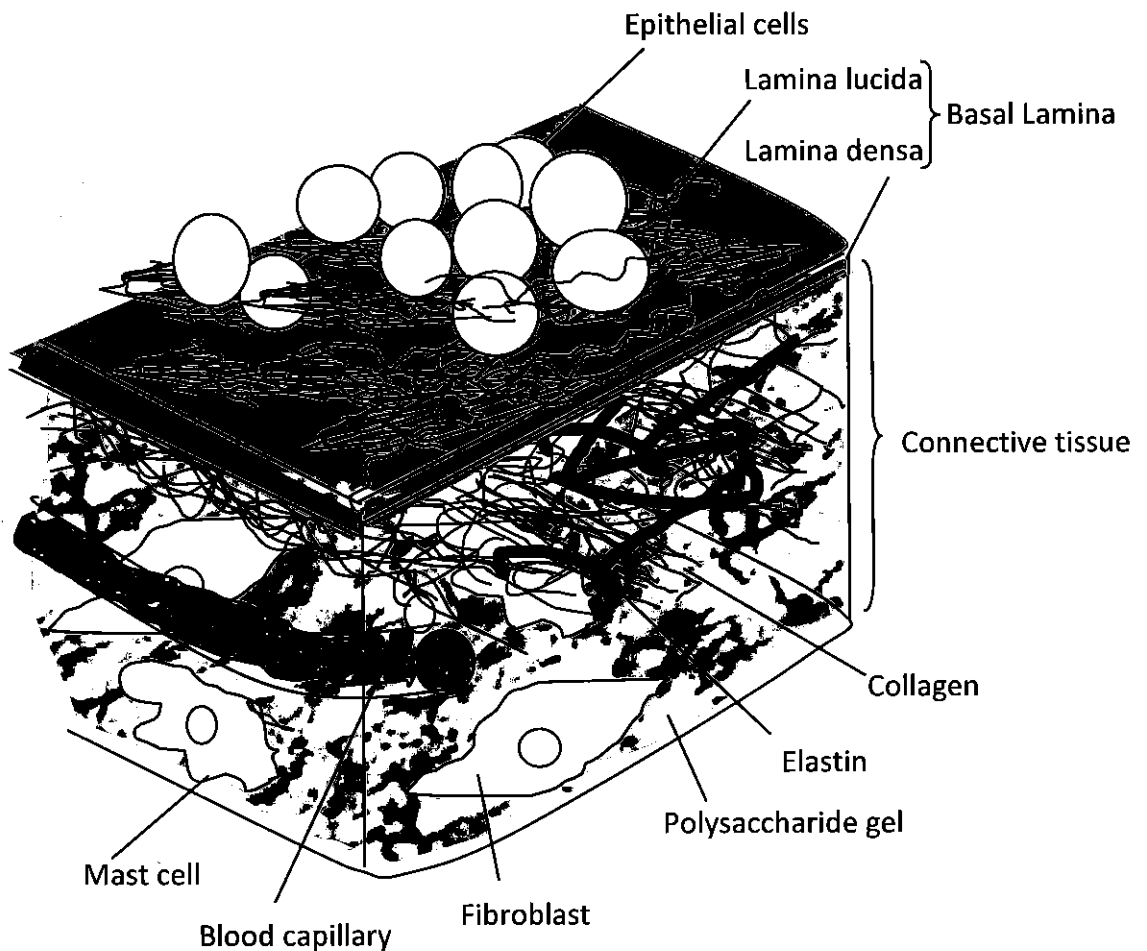


Figure 1.3. Structure of basal lamina and connective tissue

The exact composition of basal lamina varies from tissues to tissue (Pruniéras et al., 1983). A majority of the mature basal lamina consisted of type IV collage, laminin, perlecan, and entactin (Stanley et al., 1982b). During the early synthesis of basal lamina in the development of embryo, the basal lamina does not consist of collagen

type IV molecules but instead consists of a large laminin network (Turkesen et al., 1985, Pöschl et al., 2004). In the absence of collagen, laminin molecules are capable of self-assembling into a sheet in an in-vitro culture (Kirfel and Herzog, 2004, Pruniéras et al., 1983, O'Toole, 2001). Laminin has three polypeptide network that are disulfide bonded and this networks contains binding domains for collagen type IV molecules, entactin, perlecan and cell surface receptors (Beck et al., 1990). In large networks of basal lamina, laminin can directly bridge to the type IV collagen molecules which in turn, associated with type IV collagen, perlecan and entactin (Beck et al., 1990). In terms of the binding domains of laminin to the cells, fragment 1 and 8 of laminin are exposed as the adhesion sites for cell surface receptors (Aumailley et al., 1987).

1.2.3 Integrin Receptors and Focal Adhesion

The function of various types of receptors found on the surface of the cell membrane is to provide adhesion to the ECM proteins (Dzamba et al., 2001). These receptors are transmembrane proteins of a large family known as integrins. Integrins are classified as the heterodimers which are composed of two distinct chains, the α (alpha) and β (beta) subunits (Burrige et al., 1997). In cell-ECM attachment, the specific ligands in the ECM determine the type of α and β subunits of the integrins being expressed by a cell (Geiger and Bershadsky, 2001). Some examples of integrins are as given in Table 1.1. Multiple integrins exist on the cell membrane and they work co-operatively with the cell adhesion proteins in cell-cell and cell-ECM interaction (Hynes, 2002).

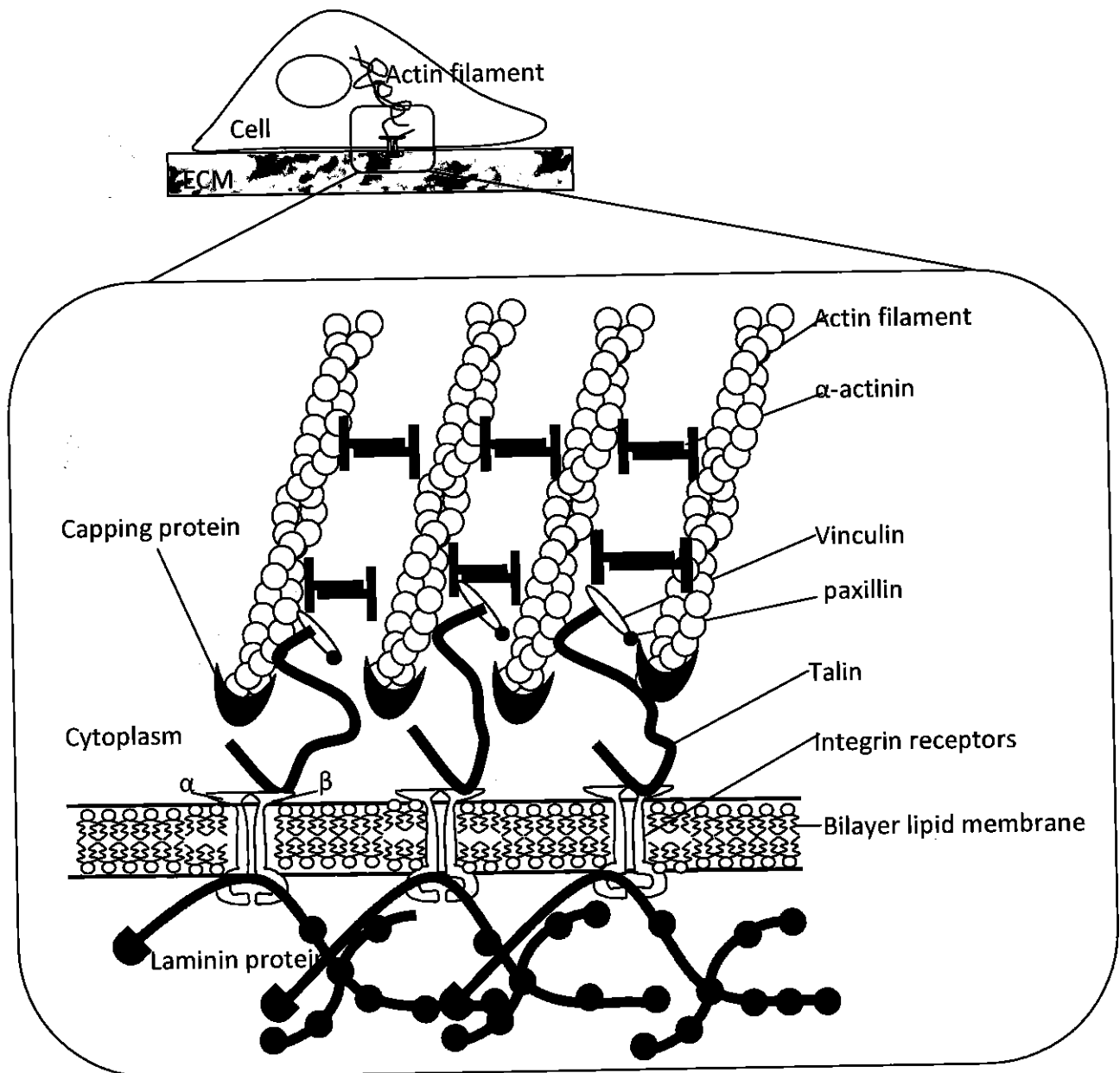


Figure 1.4. The structures of actin cytoskeleton, focal adhesion complexes, integrin receptors, and adhesion proteins.

Integrins have a dual function, that of transducing signals (either biochemical or physical) from the ECM to the cell and also the function of mediating the transmission of forces generated within the cell to the ECM (Geiger and Bershadsky, 2001, Hynes, 2002). Hence, they work as mechanosensors in sensing the stiffness of the ECM (Bershadsky et al., 2003, Rivelina et al., 2001) whilst functioning as transmembrane messenger which trigger signals in regulating cellular attachment, migration and differentiation (Dzamba et al., 2001, Geiger et al., 2001).

Table 1.1. Associated ligands receptor identified for human keratinocytes migration.

Integrins	Ligands	Reference
$\alpha 2\beta 1$	Type I Collagen	(O'Toole, 2001, Kim et al., 1992)
$\alpha 2\beta 1, \alpha 3\beta 1$	Laminin 5	(Decline and Rousselle, 2001, Kainulainen et al., 1998)
$\alpha 5\beta 1, \alpha 3\beta 1$	Fibronectin	(O'Toole, 2001, Kirfel and Herzog, 2004)

Focal adhesions (FA) or focal contacts (FC) located within the cell (Figure 1.2) are adhesion plaques which assist the actin cytoskeleton to anchor to the ECM *via* the integrin receptors (Figure 1.4). Focal adhesions consist of a number of proteins such as α -actinin, talin, paxillin and vinculin (Burrige et al., 1997, Geiger and Bershadsky, 2001, Wong, 1999) as seen in Figure 1.4. Among these protein molecules, vinculin is the major protein molecule at the sub-membrane plaque (Schwartz and DeSimone, 2008).

1.2.4 Polymerisation of Actin Filaments and Generation of Traction Force

Actin filaments of the actin cytoskeleton are the main machinery in regulating the contractility of a cell. Actin is a globular protein (Boron and Boulpaep, 2004), however, they can assemble and polymerise in a helical fashion to form filamentous actin double helix (Figure 1.5).



Figure 1.5. Assembly of globular proteins into long chain of actin filaments in helical structure.

The contractility of the non-muscle cells is dependent on the translational interactions between myosin-II and the filamentous actin (F-actin or sub unit of actin filament) (Langanger et al., 1986). Upon stimulation of cell contraction, the

phosphorylation of the F-actin allows the myosin II head to bind and sliding along the adjacent F-actin fibres in opposite directions (Peterson et al., 2004) as shown in Figure 1.6 (a-b). The mechanical actuation and phosphorylation of myosin II heads are driven by harnessing the energy released from adenosine triphosphate (ATP) when it is hydrolysed to ADP, this is regulated by myosin light chain kinase (Tan et al., 1992). This mechanism regulates the stretching and contraction of actin filaments in the longitudinal direction. To gain movements in transverse direction, α -actinin reduces the spacing between the two filaments by drawing bundles of actin filaments closer to each other (Figure 1.6c) (Pellegrin and Mellor, 2007). The collective actions of both myosin II and α -actinin in the actin filaments trigger the formation of stress fibres and cell contractility. With the binding of the actin filaments, FA and integrins receptor to the ECM, this creates a shear force exerted on the ECM, consequently, inducing cell surface traction (Lazarides and Weber, 1974, Pellegrin and Mellor, 2007).

Under 100x magnification of immunofluorescence microscopy, the stress fibres appear in a periodic "sarcomeric" organisation (Figure 1.7) are similar to the myofibrils of muscle (Peterson et al., 2004), in which the sarcomeres observed in non-muscle cells are the repeatable patterns of α -actinin (Pellegrin and Mellor, 2007).

The contractility of actin filaments bundles allows cells to actively re-structure their cell body to accommodate to the stiffness of the surrounding environment. When cells are grown on a glass cover slip, a broadly spread morphology is acquired by cells to sustain their bodies on the stiff substrate. For cells attached to a hard surface, isometric contraction and the parallel arrangement of aligned stress fibres are the dominant features of the cytoskeleton as shown in Figure 1.7 (Peterson et al., 2004).

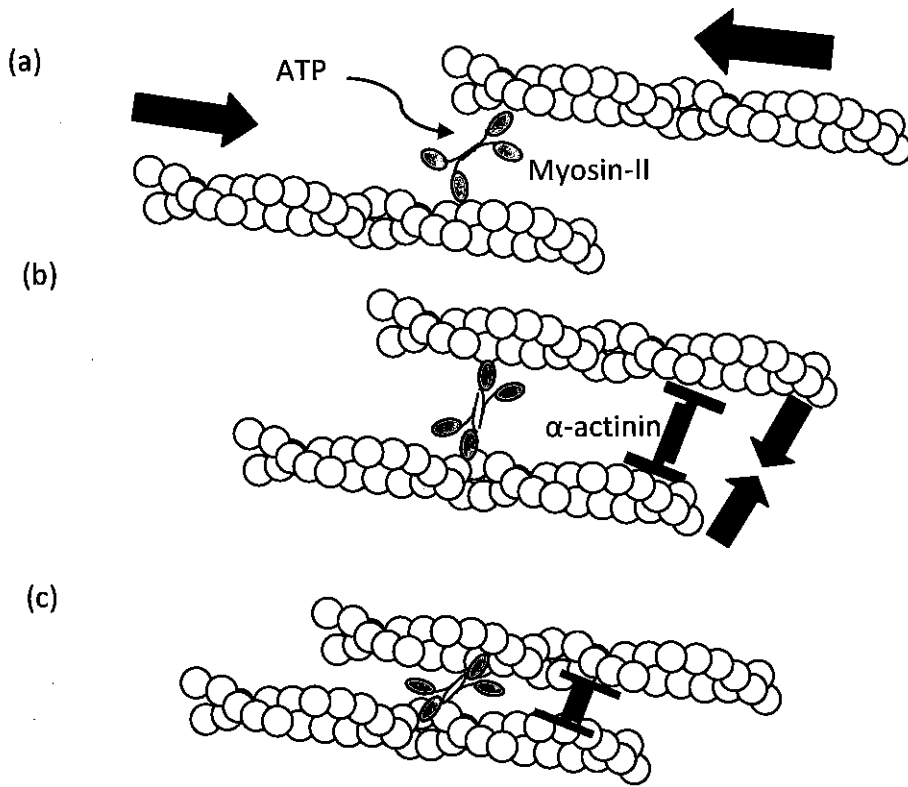


Figure 1.6. The mechanism of actin filaments contraction in bi-directions.

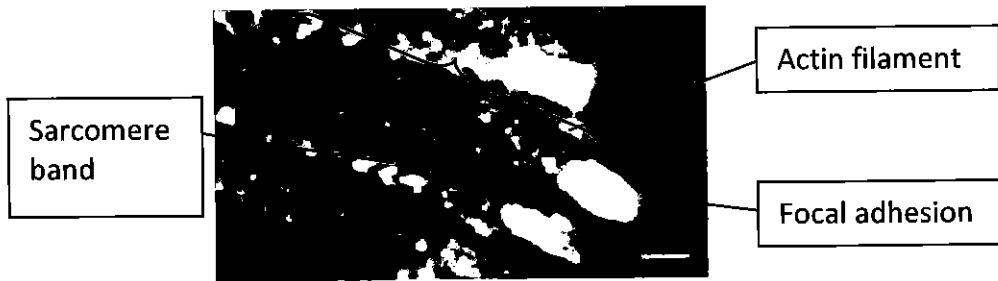


Figure 1.7. Sarcomeric appearance of the actin filament (Peterson et al., 2004). (Scale bar: 2 μ m)

Some studies (Sagvolden et al., 1999, Rivelinea et al., 2001) show that cells are very sensitive to their interface tension and this can be seen when tension is applied to a cell membrane (for example, indenting the cell membrane with a microneedle). In this example, the cell rapidly generates stress fibres at that localised region (Rivelinea et al., 2001). In resisting tension, the cell reorganises the network of filaments to adapt to the stress. Consequently, focal adhesions are stimulated and assemble into clusters

in response to the onset of the contractility (Peterson et al., 2004). A higher recruitment of stress fibres increases the size of the focal adhesions, and hence induces higher contractile forces (Goffin et al., 2006). Reversible disassembly of the focal adhesions results in a disruption in the contractility of cells (Burrige and Chrzanowska-Wodnicka, 1996).

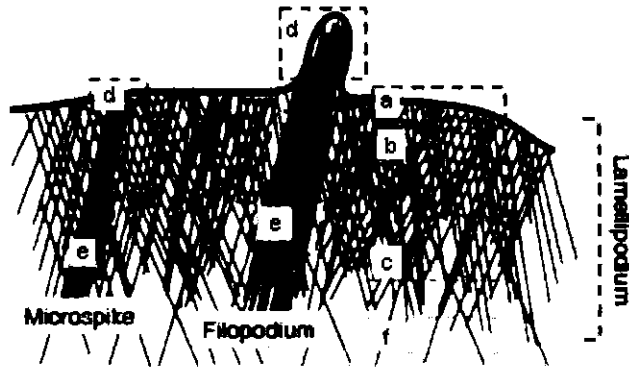


Figure 1.8. A schematic showing the sub-components of the lamellipodia and filopodia: (a) tip of lamellipodium, (b) actin meshwork, (c) region of major disassembly, (d) tip of filopodium, (e) bundle, and (f) undegraded filament which contributes to the cytoplasmic network (Small et al., 2002).

In addition to the functions of contraction, these filament networks are able to protrude and pressurise intracellularly against the cell membrane in the form of lamellipodia and filopodia. Lamellipodia contains quasi two-dimensional actin meshes that extends across and to the edge of the cell membrane (Figure 1.8a-c, f) to make contact with a surface (Small et al., 2002). Beyond the frontier of the lamellipodia, further microscopic protrusion of the membrane exists as microspikes, otherwise known as the filopodia (Figure 1.8d-e).

The assembly and disassembly of the actin filaments and associated integrin receptors are regulated by the GTPase family members (Figure 1.9) such as Rho, Rac, and cdc42 (Hall, 2005, Mackay and Hall, 1998). GTPase is an enzyme which hydrolyses guanosine triphosphate (GTP) that consists of monomeric GTP-binding proteins. These

are specialised molecular proteins that control the transduction pathways within the cell (Hall, 2005, Burridge et al., 1997). Rho triggers the bundling of actin filaments into stress fibres (Figure 1.9) (Mackay and Hall, 1998, Hall, 2005). Activation of Rac leads to the assembly of actin filaments in a meshwork at the periphery of a cell to form lamellipodia and membrane ruffles (Mackay and Hall, 1998). The third member, Cdc42 activates the actin filaments to form filopodia (Figure 1.9) (Mackay and Hall, 1998). There is also cross-talk between the monomeric G-proteins, for example, Rac can activate Rho in fibroblasts (Hall, 1998, Mackay and Hall, 1998). Hence, these signaling pathways control the structural changes that in turn are responsible for cell attachment and migration on the underlying substrate.

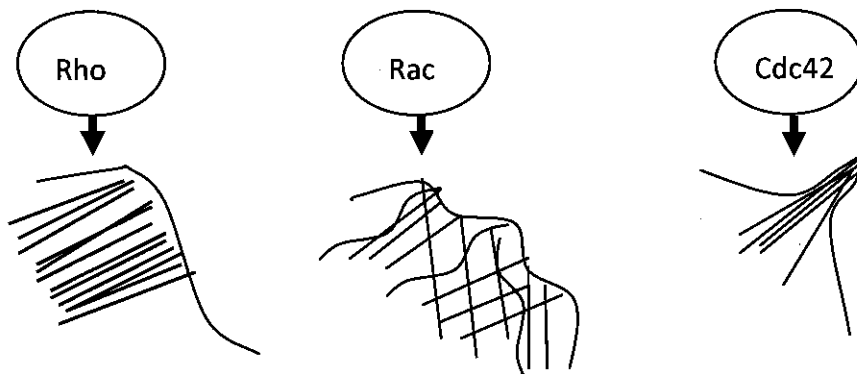


Figure 1.9. Activation of actin filaments by Rho, Rac and Cdc42

During cell migration, G-protein activates the down-stream signaling in order to elicit the formation of stress fibres, which then leads to the regulation of cell contractility. In triggering epithelial cells to change from a static to a migratory phenotype, the messaging could be regulated by cytokines such as Transforming Growth Factor Beta (TGF β). TGF β is a multifunctional cytokine which regulates many cellular process in keratinocytes such as the cell differentiation, proliferation and migration (Cross and Mustoe, 2003, Massague and Wotton, 2000). Over the cell membrane surface, TGF β binds to type II receptor (TGF β RII) which then

phosphorylates type I receptor (TGF β RI) as shown in Figure 1.10. TGF β RI and TGF β RII are both obligate heteromeric transmembrane receptors (Wrana, 1998). The phosphorylation of TGF β RI leads to phosphorylation of Receptor activated-Drosophila gene Mothers against dpp (R-Smads) (as seen in Figure 1.10) with members termed Smad2 and Smad3 that continue to form complexes with Smad4 (Massague and Wotton, 2000). The complex of R-Smad and co-Smads translocates to the nucleus where these transcription factors regulate the target gene and activations of subsequent cellular processes (Massague and Wotton, 2000, O'kane and Ferguson, 1996).

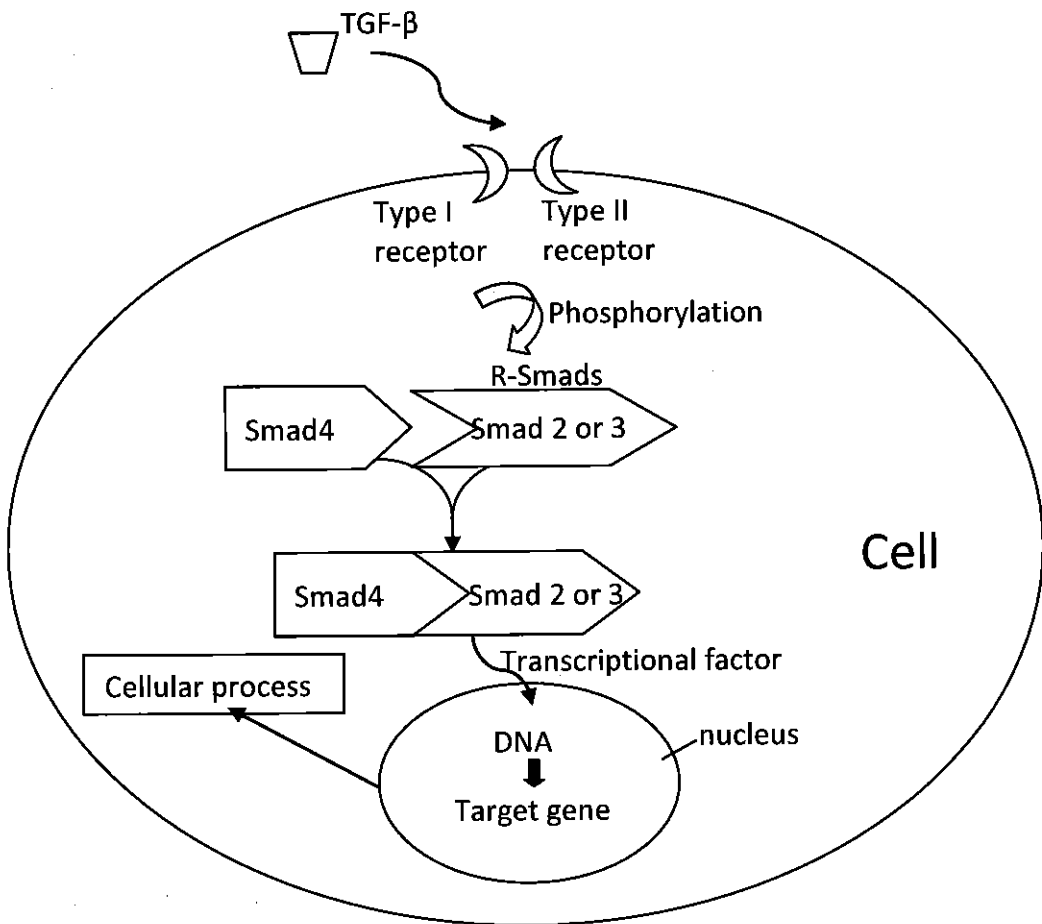


Figure 1.10. The intracellular signaling pathway of TGF- β .

The family of cytokine such as TGF- β 1, TGF- β 2 and TGF- β 3. Particularly, TGF- β 1 which is isolated from human platelets, human placenta and bovine kidney is an

attractive cytokine because of the contradicting role of the cytokine in wound therapy and abnormal epidermis formation (for example, scar formation and psoriasis) (Li et al., 2004a, Zhang et al., 2003, Gailit et al., 1994) which is still not clearly understood. However, treatment of keratinocyte in in-vitro cultures with TGF- β 1 > 10 ng/ml was reported to promote cell motility, and rapidly increase the Rho activity and β -actin formation (Decline et al., 2003, Coffey et al., 1988, Bhowmick et al., 2001, Shen et al., 2001).

Contractility of cells is the basic causal event which regulates the integrity of tissue (Deugnier et al., 2002, Heida et al., 1996), cytokinesis and morphogenesis (Singer et al., 1999, Horwitz and Parsons, 1999, Kirfel and Herzog, 2004). Due to the importance of the cellular contractility, many polymer based cell traction force measurement techniques have been developed to probe the mechanics and physiological changes that occur in contracting cells (mainly fibroblasts).

Research in mechanobiological measurement systems is expanding fast. Seven methods of probing cells mechanically have been developed as shown in Figure 1.11. These methods are classified as the atomic force microscopy (AFM) nano-indentation, magnetic twisting cytometry, micropipette aspiration, optical trapping, shear flow, soft substrate stretching (Bao and Suresh, 2003) and quartz crystal microbalance systems (Pax et al., 2005, Kang and Muramatsu, 2008). Except for the use of soft substrate techniques, the majority of techniques is either very time consuming or requires considerable investment in expensive equipment, and thus these techniques are not suitable for high throughput drug screening. In comparison, the systems based around soft substrates seem to be the most promising tool for pharmacology application because of their low development cost and potential in high throughput screening.

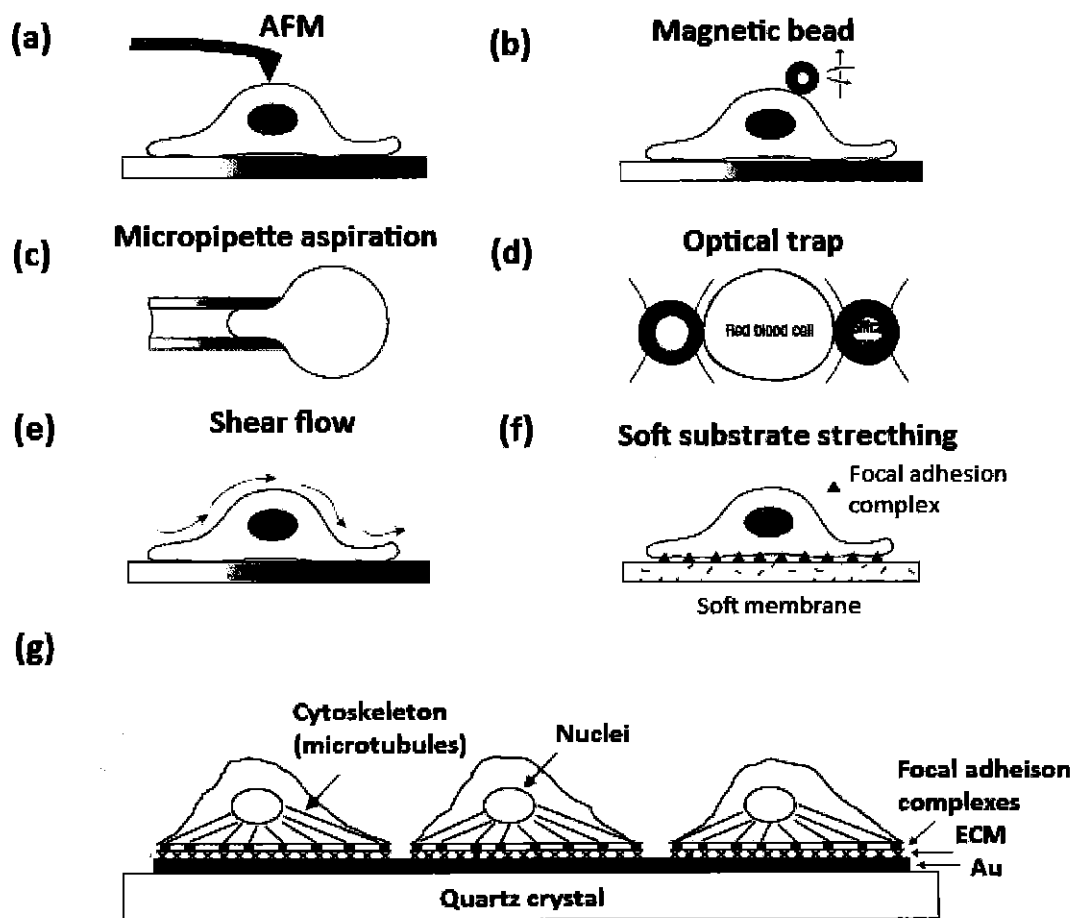


Figure 1.11. Seven experimental techniques used in probing mechanical response of a cell. (a) Atomic force microscopy (b) magnetic twisting cytometry, (c) micropipette aspiration, (d) optical trapping, (e) shear flow, (f) soft substrate stretching (Bao and Suresh, 2003) and quartz crystal (Marx et al., 2005).

The most commonly used soft materials to monitor cell forces are silicone rubber, collagen sheets, polyacrylamide (PAA) and polydimethylsiloxane (PDMS). For example, measuring the shrinkage of a collagen sheet caused by adherent contracting cells is a widely used technique. This type of soft substrate system was applied to assess the effect of Endothelin-1 on smooth muscle cells (Dallot et al., 2003) but it does not provide any information about the contractility characteristic of cells such as morphology changes, force distribution, cell mechanics and traction pattern for single cells. Therefore, more sensitive methods are required to probe the biomechanics of a single cell.

1.2.5 Force Sensor Based on Silicon Sheet

The first use of a thin flexible silicon sheet in monitoring cell traction force can be traced back to the work of (Harris et al., 1980). Buckling effects were observed on a thin sheet of silicon rubber seeded with chicken heart fibroblasts as shown in Figure 1.12a. Although fibroblast induced long lasting wrinkles on the silicone substrate, the most intense indentations did not correlate with the focal contact points (Hinz and Gabbiani, 2003). In order to measure the traction force correlated with the contraction activity of the α -smooth muscle actin, the indentation should be formed at the focal contacts where the anchoring of actin filament heads produce the most abundant stress. Numerous efforts have been made to improve the sensitivity and resolution of this material by increasing the flexibility of the silicon sheet by ultraviolet light treatment (Burton and Taylor, 1997). However, the enhancement on the flexibility of the silicon sheet did not significantly improve the efficiency in measurement (for example, isolation of localised stress) (Figure 1.12b) (Beningo, 2002).

The silicon sheet used for detection of cell forces is based on a continuum. This technique does not limit the cell spreading but allows dispersal of cells focal contacts and distribution of cell traction force in arbitrary directions (Beningo, 2002). However, there are two problems arising from this technique. Firstly, the quantification of forces involves the direct use of a longitudinal deformation line in which, the force was calculated by multiplying the length of the longitudinal deformation line (wrinkle) by the stiffness of the material (Oliver et al., 1995). The stiffness of the silicon substrate used in previous work was determined by measuring the lengths of the wrinkles induced by a calibrated deflection force (Burton et al., 1999).

- ABBOTT, N. L., N., L., MURPHY, C. J., CHING, L.-L. & JANG, C.-H. (2005) Engineering interfaces to cells using synthetic liquid crystals. *European Cells and Materials* 10, CS1.
- ABSOLOM, D., R., LAMBERTI, F., V., POLICOVA, Z., ZINGG, W., OSS, C., J. VAN, & NEUMANN, A. W. (1983) Surface Thermodynamics of Bacterial Adhesion. *Applied and Environmental Microbiology*, 46, 90-97.
- ADDAE-MENSAH, K. & WIKSWO, J. (2008) Measurement techniques for cellular biomechanics in vitro. *Experimental Biology and Medicine (Maywood)*, 233, 792-809.
- AHEARNE, M., YANG, Y., EL HAJ, A. J., THEN, K. Y. & LIU, K.-K. (2005) Characterizing the viscoelastic properties of thin hydrogel-based constructs for tissue engineering applications. *Journal of The Royal Society of Interface*, 2, 455-463.
- AKIHO, H., BLENNERHASSETT, P., YIKANG, D. & COLLINS, S. M. (2002) Role of IL-4, IL-13, and STAT6 in inflammation-induced hypercontractility of murine smooth muscle cells. *American journal of physiology*, 45, G226-G232.
- ALBERTS, A. S. & TREISMAN, R. (1998) Activation of RhoA and SAPK/JNK signalling pathways by the RhoA-specific exchange factor mNET1. *The EMBO Journal*, 17, 4075-4085.
- ALBERTS, B., JOHNSON, A., LEWIS, J., RAFF, M., ROBERTS, K. & WALTER, P. (2002) *Molecular Biology of the Cell*, Garland Science.
- ALCANTARA, M. R. & FERNADES JR., E. G. (2002) Twenty years of research on cholesteric lyotropic liquid crystals at the chemistry institute of the University of Sao Paulo. *Brazilian Journal of Physics*, 32, 509-515.
- ANTCZAK, S. & ANTCZAK, G. (2001) *Cosmetics unmasked*, Thorsons, HarperCollins.
- ASHCROFT, G. S., YANG, X., GLICK, A. B., WEINSTEIN, M., LETTERIO, J. L., MIZEL, D. E., ANZANO, M., GREWELL-WILD, T., WAHI, S. M., DENG, C. & ROBERTS, A. B. (1999) Mice lacking Smad3 show accelerated wound healing and an impaired local inflammatory response. *Nature Cell Biology*, 1, 260-266.
- ASHER, S. A. & PERSHAN, P. S. (1979) Alignment and defect structures in oriented phosphatidylcholine multilayers. *Biophysical Journal* 27, 393-421.
- AUMAILLEY, M., NURCOMBEG, V., EDGAR, D., PAULSSON, M. & TIMPL, R. (1987) The cellular Interactions of laminin fragments. *The Journal of Biological Chemistry*, 262, 11532-11538.
- BALABAN, N., SCHWARZ, U., RIVELINE, D., GOICHBERG, P., TZUR, G., SABANAY, I., MAHALU D, S. S., BERSHADSKY, A., ADDADI, L. & GEIGER, B. (2001) Force and focal adhesion assembly: a close relationship studied using elastic micropatterned substrates. *Nature Cell Biology*, 3.
- BALABAN, N. Q., SCHWARZ, U. S. & GEIGER, B. (2006) Measurement of cellular contractile forces using patterned elastomer. IN CELIS, J. E. (Ed.) *Cell biology: a laboratory handbook, Volume 1*. Elsevier.
- BAO, G. & SURESH, S. (2003) Cell and molecular mechanics of biological materials. *Nature Materials*, 2, 715-725.
- BAREL, A., COURAGE, W. & CLARYS, P. (1995) Suction method for measurement of skin mechanical properties: the cutometer. IN SERUP, J. A. J., G.B.E. (Ed.) *Handbook of Non-Invasive Methods and the skin*. . Boca Raton, CRC Press.
- BARNES, H. A., HUTTON, J. F. & WALTERS, K. (1989) *An introduction to rheology*, Amsterdam, Elsevier.
- BARTKOVA, J., GRØN, B., DABELSTEEN, E. & BARTEK, J. (2003) Cell-cycle regulatory proteins in human wound healing. *Archives of Oral Biology*, 48, 125-132.

- BASAPPA, G., SUNEEL, KUMARAN, V., NOTT, P. R., RAMASWAMY, S., NAIK, V. M. & ROUT, D. (1999) Structure and rheology of the defect-gel states of pure and particle-dispersed lyotropic lamellar phases. *The European Physical Journal B*, 12, 269-276.
- BAUMANN, H. & DOYLE, D. (1979) Effect of trypsin on the cell surface proteins of hepatoma tissue culture cells. *The Journal of Biological Chemistry*, 254, 3935-3946.
- BECK, K., HUNTER, I. & ENGEL, J. (1990) Structure and function of laminin: anatomy of a multidomain glycoprotein. *The FASEB journal*, 4, 148-160.
- BECKER, W., HETTICH, B. S. & HOENICKE, P. (2001) Toxicological and ecotoxicological investigations of liquid crystals and disposal of LCDs IN KGAA, M. (Ed. *Liquid Crystals Division and Institute of Toxicology 64271*. Darmstadt, Germany.
- BEHREND, J. C. & FERTIG, N. (2007) Neuromethods. IN WALZ, W. (Ed.) *Patch clamp analysis*. 2nd ed.
- BENINGO, K., LO, C. & WANG, Y. (2002) Flexible polyacrylamide substrata for the analysis of mechanical interactions at cell-substratum adhesions. *Methods Cell Biol.*, 69, 325-339.
- BENINGO, K. A. (2002) Flexible substrata for the detection of cellular traction forces. *Trends in Cell Biology*, 12, 79-84.
- BENNETT, M. R., M & PETTIGREW, A. G. (1974) The formation of synapses in striated muscle during development. *Journal of Physiology*, 241, 515-545.
- BERGHAUSEN, J., ZIPFEL, J., DIAT, O., NARAYANAN, T. & RICHTERING, W. (2000) Lamellar phases under shear : variation of the layer orientation across the couette gap. *Phys. Chem. Chem. Phys*, 2, 2623-3626.
- BERSHADSKY, A., BALABAN, N. & GEIGER, B. (2003) Adhesion-dependent cell mechanosensitivity. *Annu Rev Cell Dev Biol.*, 19, 677-695.
- BETZ, W. J. & SAKMANN, B. (1971) "Disjunction" of frog neuromuscular synapses by treatment with proteolytic enzymes. *Nature New Biology*, 232, 94-95.
- BHOWMICK, N. A., GHIASSI, M., BAKIN, A., AAKRE, M., LUNDQUIST, C. A., ENGEL, M. E., ARTEGA, C. L. & MOSES, H. L. (2001) Transforming growth factor- β 1 mediates epithelial to mesenchymal transdifferentiation through a RhoA-dependent mechanism. *Molecular Biology of the Cell*, 12, 27-36.
- BIRCHALL, L. S., ULIJN, R. V. & WEBB, S. J. (2008) A combined SPS-LCD sensor for screening protease specificity. *Chemistry Communication*, 25, 2861-2863.
- BITAR, K. N. & MAKHLOUF, G. M. (1985) Measurements of function in isolated single smooth muscle cells. *Am J Physiol Gastrointest Liver Physiol* 250, G357-360.
- BOLAND, S., BOISVIUX-ULRICH, E., HOUCINE, O., BAEZA-SWUIBAN, A., POUCHELET, M., SCHOEVAERT, D. & MARANO, F. (1996) TGF β 1 promotes actin cytoskeleton reorganization and migratory phenotype in epithelial tracheal cells in primary culture. *Journal of cell Science*, 109, 2207-2219.
- BOLOGNIA, J. L., JORIZZO, J. L. & RAPINI, R. P. (2004) *Dermatology*, Spain, Mosby.
- BORON, W. F. & BOULPAEP, E. L. (2004) *Medical Physiology: A Cellular And Molecular Approach*, Elsevier/Saunders.
- BOUTELIER, D., SCHRANK, C. & CRUDEN, A. (2008) Power-law viscous materials for analogue experiments: New data on the rheology of highly-filled silicone polymers. *Journal of Structural Geology* 30 341-353.
- BOYD, R. H. (1993) *The science of polymer molecules: an introduction concerning the synthesis, structure and properties of the individual molecules that constitute polymeric materials.* , Cambridge, Camb. U. P.

- BRAKE, J. M., DASCHNER, M. K., LUK, Y.-Y. & ABBOTT, N. L. (2003) Biomolecular interactions at phospholipid-decorated surfaces of liquid crystals. *Science*, 302, 2094-2097.
- BRITLAND, S., PERRIDGE, C., DENYER, M., MORGAN, H., CURTIS, A. & WILKINSON, C. (1996) Morphogenetic guidance cues can interact synergistically and hierarchically in steering nerve cell growth. *Experimental Biology Online*, 1, 1-15.
- BUCK, C. A. & HORWITZ, A. F. (1987) Cell surface receptors for extracellular matrix molecules. *Annual Review of Cell Biology*, 3, 179-205.
- BURRIDGE, K., CHRZANOWSKA-WODENICKA, M. & ZHONG, C. (1997) Focal adhesion assembly. *Trends in Cell Biology*, 7, 342-347.
- BURRIDGE, K. & CHRZANOWSKA-WODNICKA, M. (1996) Focal adhesions, contractility and signaling. *Annual Review of Cell and Developmental Biology*, 12 463-519
- BURRIDGE, K., FATH, K., KELLY, T., NUCKOLLS, G. & TURNER, C. (1986) Focal adhesions: transmembrane junctions between the extracellular matrix and the cytoskeleton. *Annual Review of Cell Biology*, 4, 487-525.
- BURTON, K., PARK, J. H. & TAYLOR, D. L. (1999) Keratocytes generate traction forces in two phases. *Molecular Biology of the Cell*, 10, 3745-3769.
- BURTON, K. & TAYLOR, D. L. (1997) Traction forces of cytokinesis measured with optically modified substrata. *Nature*, 385, 450-454.
- BUSATO, A. P., RIECHER, F., DOMINGUES, R. & SILVEIRA, J. L. M. (2009) Rheological properties of thermally xyloglucan gel from the seeds of *Hymenaea courbaril*. *Materials Science and Engineering C*, 29, 410-414.
- CAMPBELL, B. H., CLARK, W. W. & WANG, J. H.-C. (2003) A multi-station culture force monitor system to study cellular contractility *Biomechanics*, 36, 137-140.
- CAVEY, M. & LECUIT, T. (2009) Molecular bases of cell-cell junctions stability and dynamics. *Cold Spring Harbor Perspective of Biology*, 1, 1-18.
- CHAKRABARTY, K., HEATON, M., DALLEY, A., DAWSON, R., FREEDLANDER, E., KHAW, P. & MAC NEIL, S. (2001) Keratinocyte-driven contraction of reconstructed human skin. *Wound Repair Regeneration*, 9, 95-106.
- CHANDRASEKHAR, S. (1992) Liquid Crystals. *Cambridge University Press, Second Edition*, 1, 12.
- CHENG, L.-L., LUK, Y.-Y., CHRISTOPHER, J. M., A. ISRAEL, B. & ABBOTT, N. L. (2005) Compatibility of lyotropic liquid crystals with virus and mammalian cells that support the replication of virus. *Biomaterials* 26, 7173-7182.
- CHOI, M. C., PFOH, T., WEN, Z., LI, M. Y., KIM, W., ISRAELACHVILLI, J. N. & SAFINYA, C. R. (2004) Ordered patterns of liquid crystal toroidal defects by microchannel confinement. *Proceedings of the National Academy Sciences of the United States of America*, 101, 17340-17344.
- CLEARY, E. G. & GIBSON, M. A. (1983) Elastin-associated microfibrils and microfibrillar proteins. *International Review of Connective Tissue Research*, 10, 97-209.
- CLOYD, J. M., MALHOTRA, N. R., WENG, L., CHEN, W., MAUCK, R. L. & ELLIOTT, D. M. (2007) Material properties in unconfined compression of human nucleus pulposus, injectable hyaluronic acid-based hydrogels and tissue engineering scaffolds. *European Spine Journal*, 16, 1892-1898.
- COFFEY, R. J., BASCOM, C. C., SIPES, N. J., GRAVES-DEAL, R., WEISSMAN, B. E. & MOSES, H. (1988) Selective inhibition of growth-related gene expression in murine keratinocytes by transforming growth factor β . *Molecular and Cellular Biology*, 8, 3088-3093.

- COHEN, L. B. & SALZBERG, B. M. (1978) *Optical measurement of membrane potential*, Berlin-Heidelberg, Springer.
- COLLINGS, P. J. (2002) *Liquid crystals: nature's delicate phase of matter*, Princeton University Press.
- COLLINGS, P. J. & PATEL, J. S. (1997) *Handbook of Liquid Crystal Research*, Oxford University Press, Oxford.
- CRAMER, L. P. (2010) Forming the cell rear first: breaking cell symmetry to trigger directed cell migration. *Nature Cell Biology*, 12, 628-632.
- CRANFIELD, P. & HOFFMAN, B. (1958) Electrophysiology of single cardiac cells. *Physiological Reviews*, 38, 41-76.
- CROSS, K. J. & MUSTOE, T. A. (2003) Growth factors in wound healing. *Surgical Clinics of North America*, 83, 531-545.
- CURTIS, A. S. G. (2004) Small is beautiful but smaller is the aim: review of a life of research. *European Cells and Materials*, 8, 27-36.
- DALLOT, E., POUCHÉLET, M., GOUHIER, N., CABROL, D., FERRÉ, F. & BREUILLER-FOUCHÉ, M. (2003) Contraction of cultured human uterine smooth muscle cells after stimulation with endothelin-1 *Biology of Reproduction*, 68, 937-942.
- DECLINE, F., OKAMOTO, O., MALLEIN-GERIN, F., HELBERT, B., BERANUD, J., RIGAL, D. & ROUSSELLE, P. (2003) Keratinocyte motility induced by TGF-beta1 is accompanied by dramatic changes in cellular interactions with laminin 5. *Cell motility and the cytoskeleton*, 54, 64-80.
- DECLINE, F. & ROUSSELLE, P. (2001) Keratinocyte migration requires alpha2beta1 integrin mediated interaction with the laminin 5 gamma 2 chain. *Journal of Cell Science*, 114, 811-823.
- DELVOYE, P., WILQUET, P., LEVÊQUE, J., NUSGENS, B. & LAPIÈRE, C. (1991) Measurement of mechanical forces generated by skin fibroblasts embedded in a three-dimensional collagen gel. *Investigative Dermatology*, 97, 898-902.
- DEMBO, M., OLIVER, T., ISHIHARA, A. & JACOBSON, K. (1996) Imaging the traction stresses exerted by locomoting cells with the elastic substratum method. *Biophysical Journal*, 70, 2008-2022.
- DENEFLEA, J.-P., LECHAIREA, J.-P. & ZHUA, Q.-L. (1987) Cultured epidermis influences the fibril organization of purified type I collagen gels *Tissue and Cell*, 19, 469-478.
- DEUGNIER, M.-A., TEULIÈRE, J., FARALDO, M. M., THIERY, J. P. & GLUKHOVA, M. (2002) The importance of being a myoepithelial cell. *Breast Cancer Research* 4.
- DIKING, I. (2003) *Textures of Liquid Crystals*, Wiley-VCH.
- DIMITRIADIS, E. K., HORKAY, F., MARESCA, J., KACHAR, B. & CHADWICK, R. S. (2002) Determination of Elastic Moduli of Thin Layers of Soft Material Using the Atomic Force Microscope. *Biophysical Journal*, 82, 2798-2810.
- DIRIDOLLOU, S., PATAT, F., GENS, F., VAILLANT, L., BLACK, D., LAGARDE, J., GALL, Y. & BERSON, M. (2000) In vivo model of the mechanical properties of the human skin under suction. *Skin Research and Technology*, 6, 214-221.
- DISCHER, D. E., JANMEY, P. & WANG, Y.-L. (2005) Tissue cells feel and respond to the stiffness of their substrate. *Science*, 310, 1139-1143.
- DOERNER, M. F. & NIX, W. D. (1986) A method for interpreting the data from depth-sensing indentation instruments. *Journal of Material Research*, 1, 601-609.
- DOLE, M. (1941) *The glass electrode : methods, applications and theory*, Wiley.
- DONALD, B. J. M. (2007) *Practical stress analysis with finite elements*, Dublin, Glasnevin publishing.